

## Sensitive measurements using cold atoms

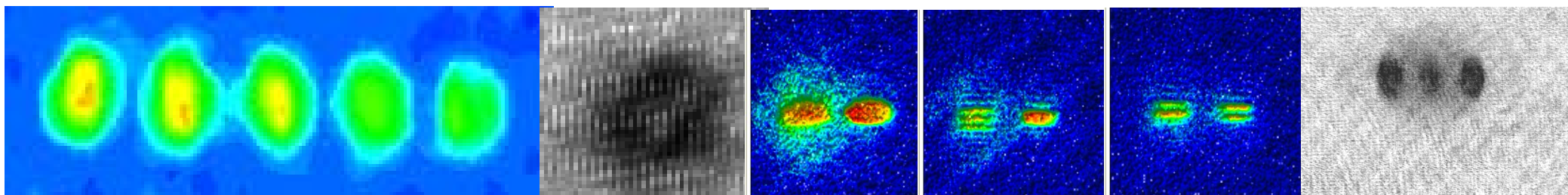
冷却原子を用いた精密計測

Department of physics, Gakushuin Univerisity

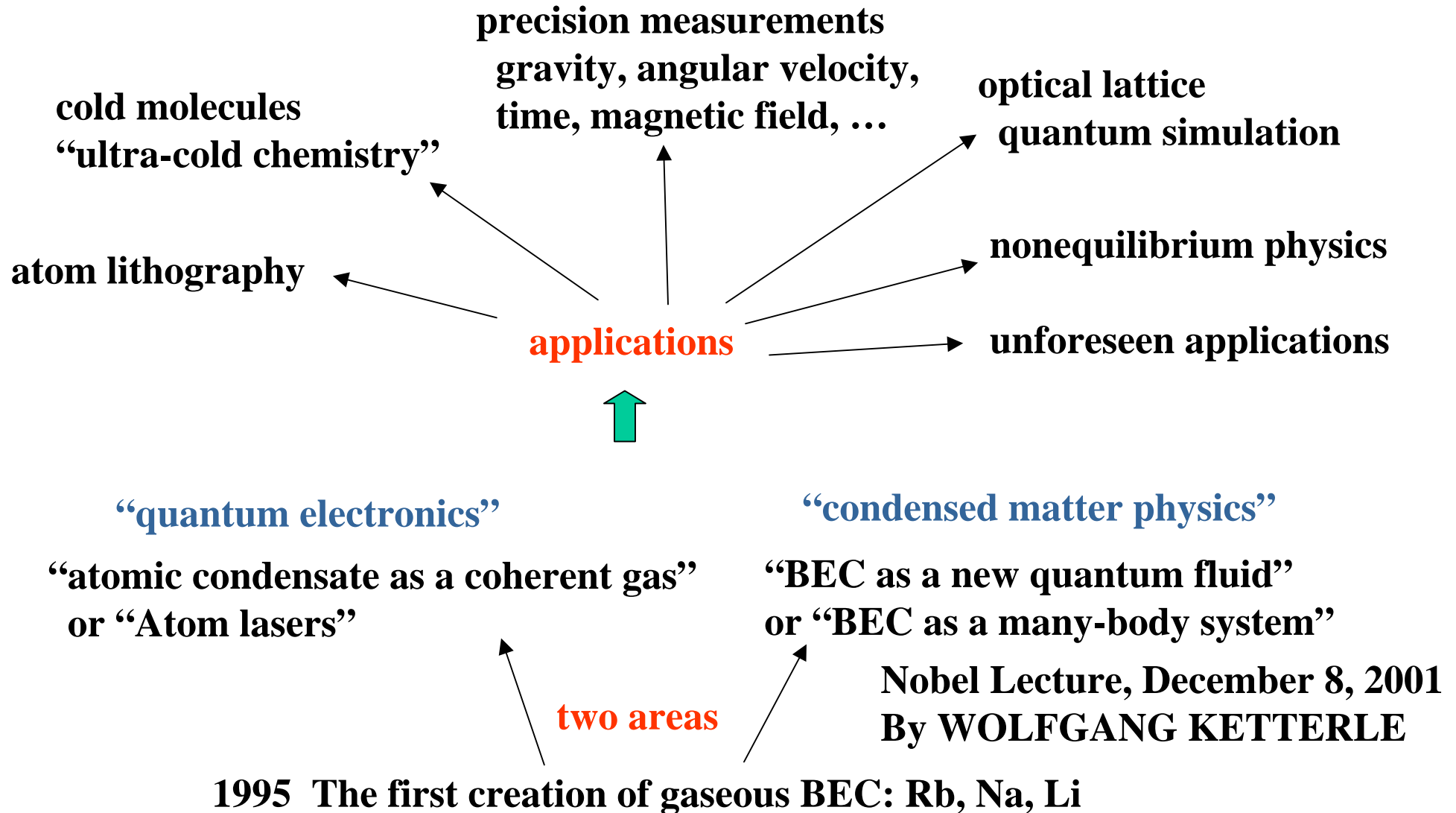
学習院大学理学部物理学科

Takuya Hirano

平野 琢也

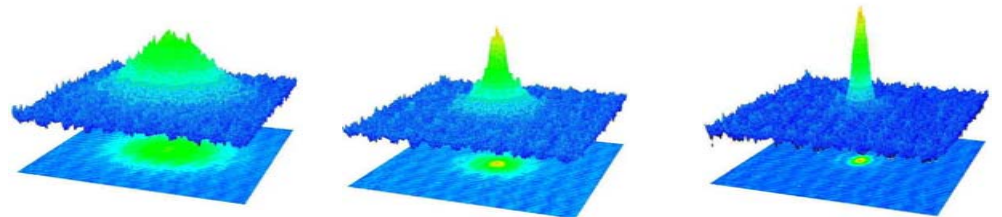


# Research on gaseous BEC



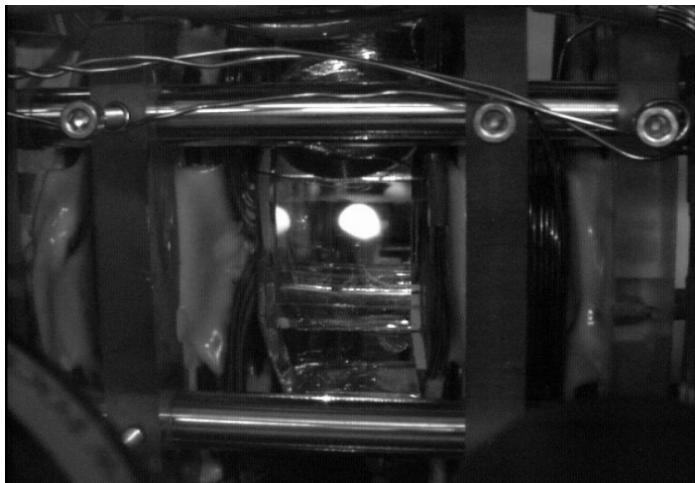
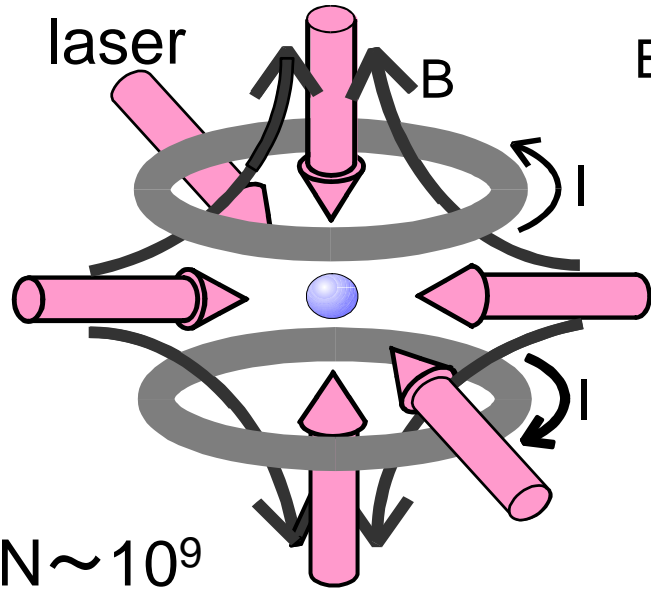
# Outline

1. Introduction
2. A brief review of atomic BEC
3. Atomic magnetometer
4. Magnetometer using BEC
5. Quantum magnetometer

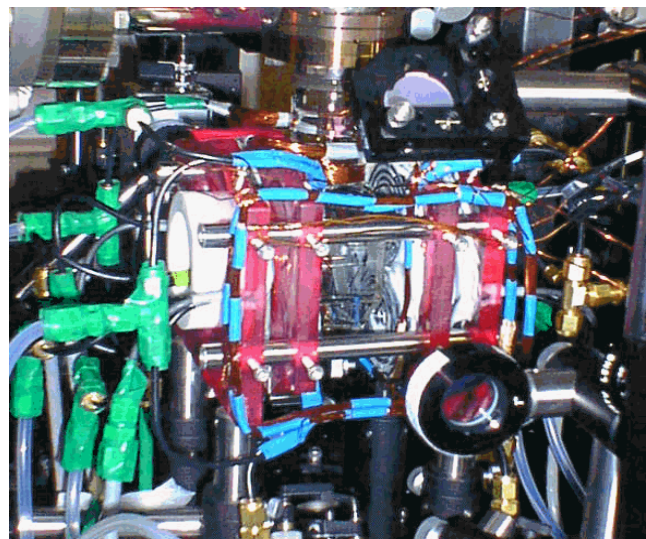
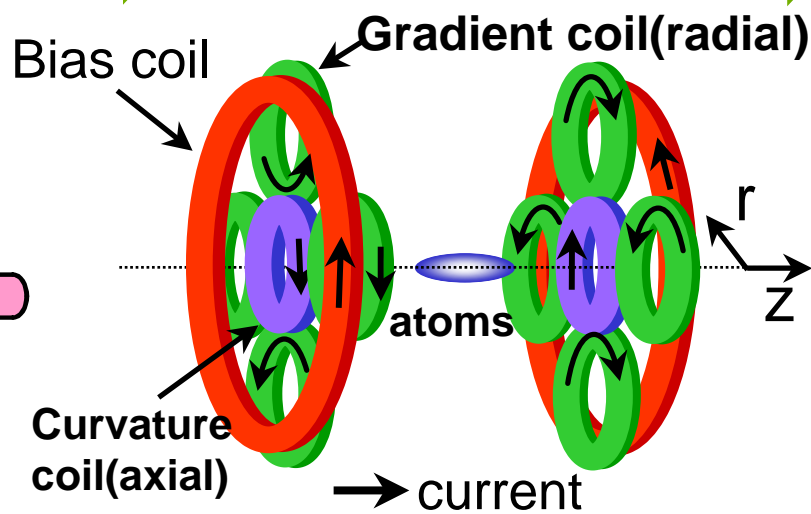


# Making of atomic BEC

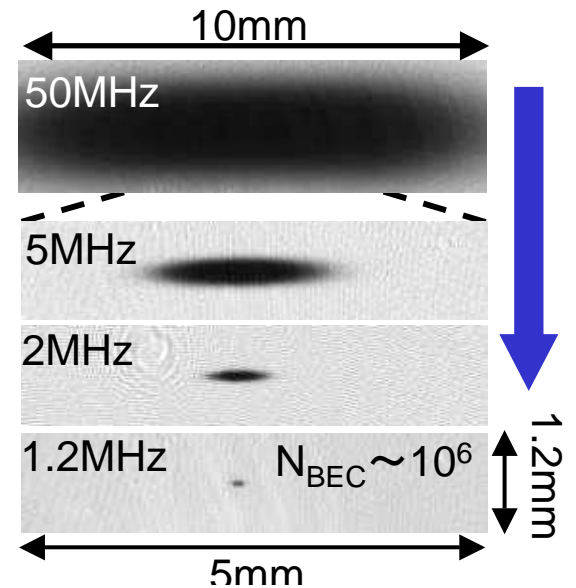
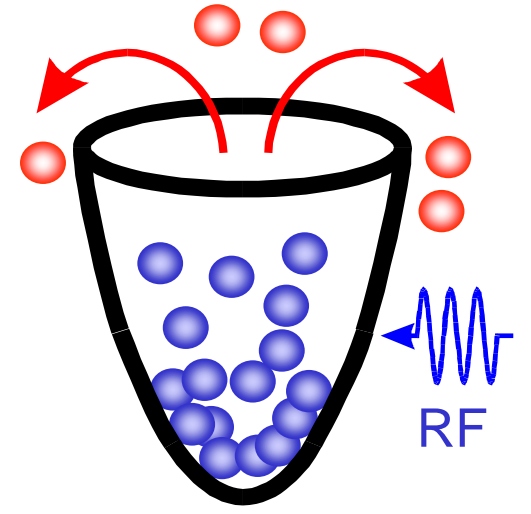
Magneto-Optical Trap(MOT)



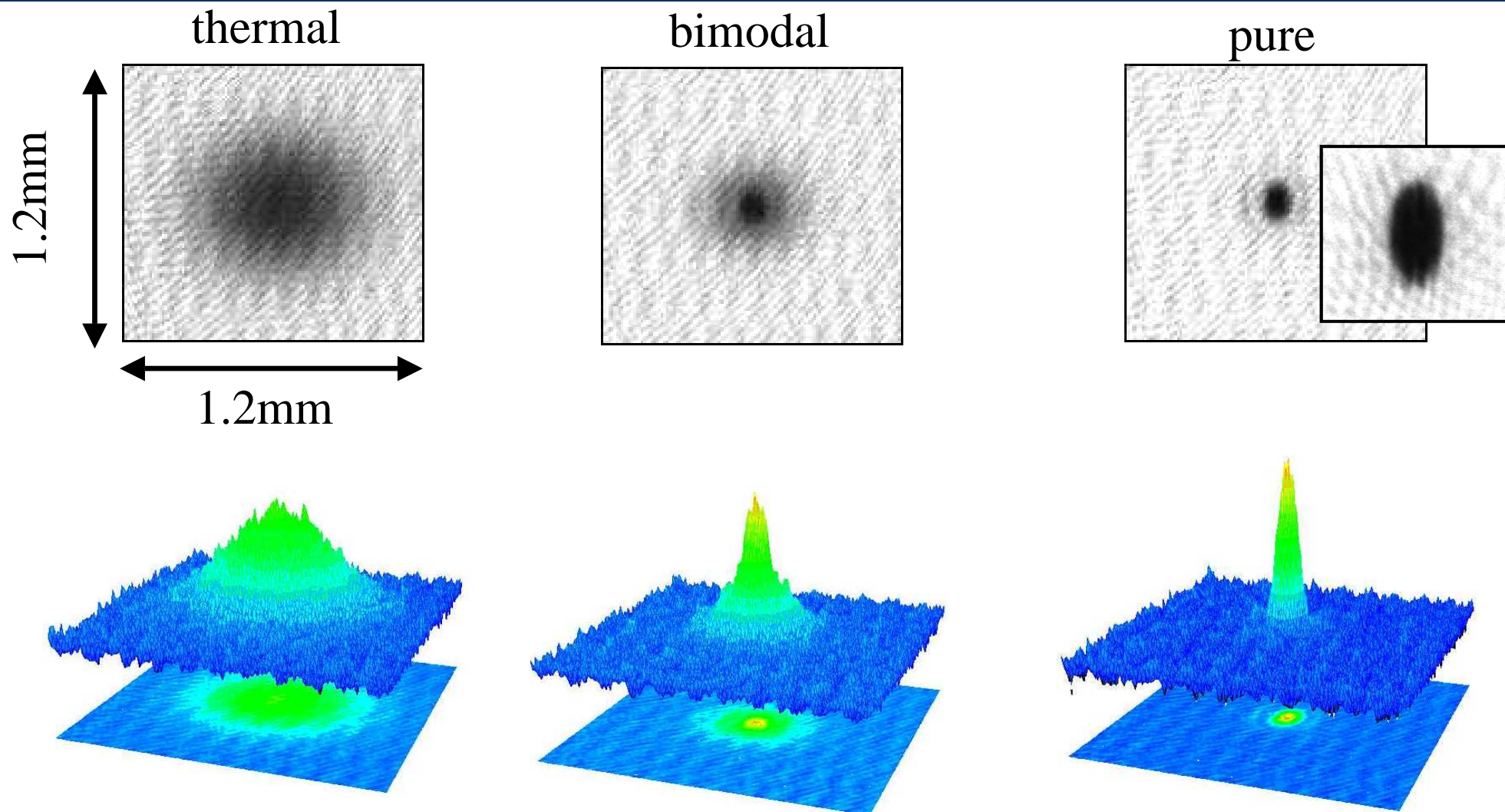
Magnetic trap



Evaporative cooling

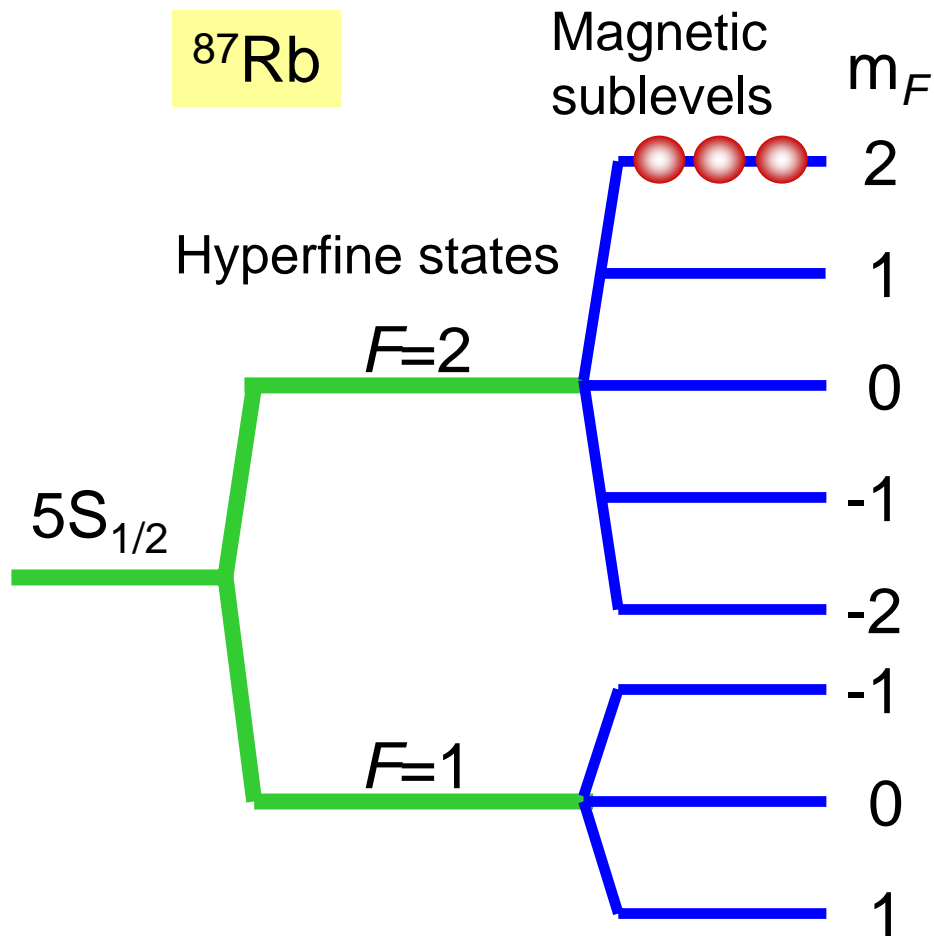


# Time Of Flight measurement of atomic BEC

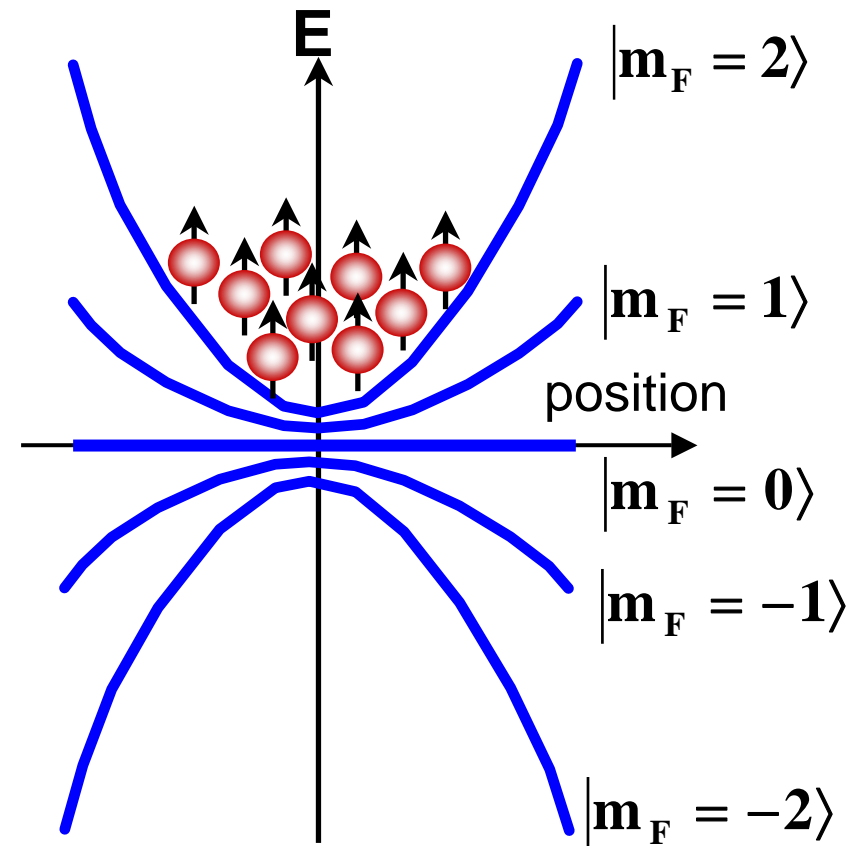


# Atoms in a magnetic trap

No spin degrees of freedom in a Magnetic trap

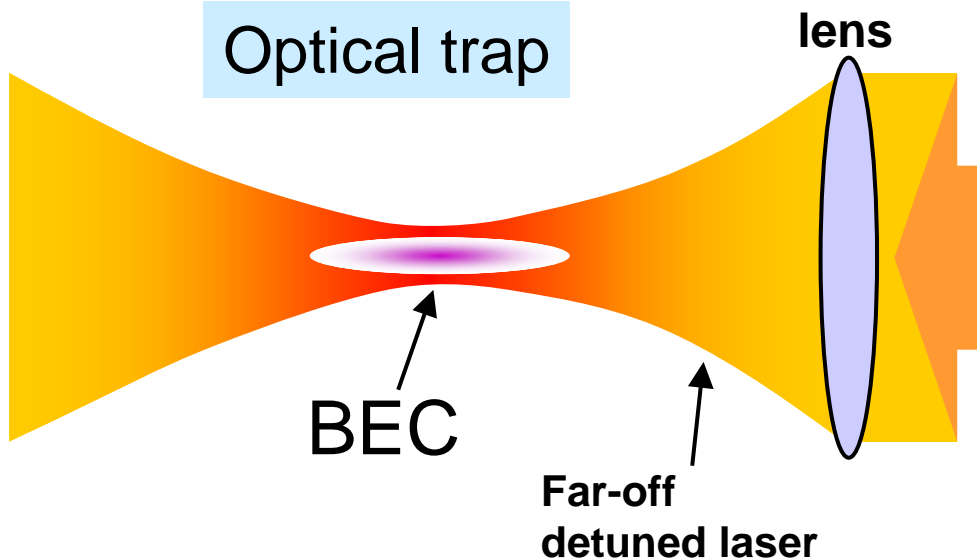


Magnetic potential for  $F=2$



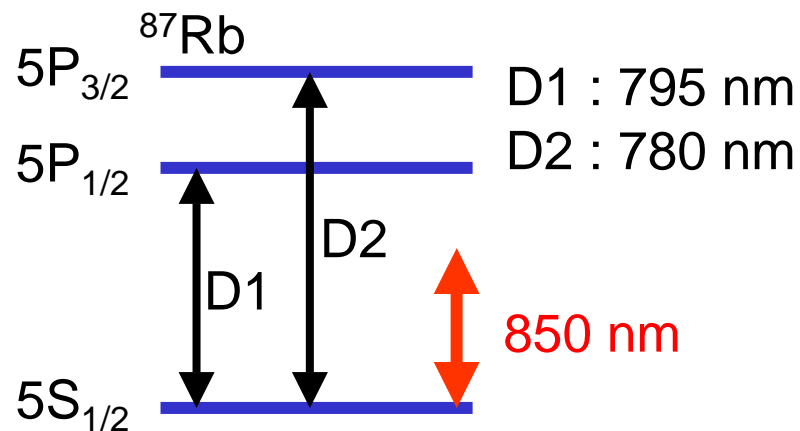
# Atoms in an optical trap

## Optical trap potential



$$U = -\frac{1}{2}\alpha \cdot |E|^2$$

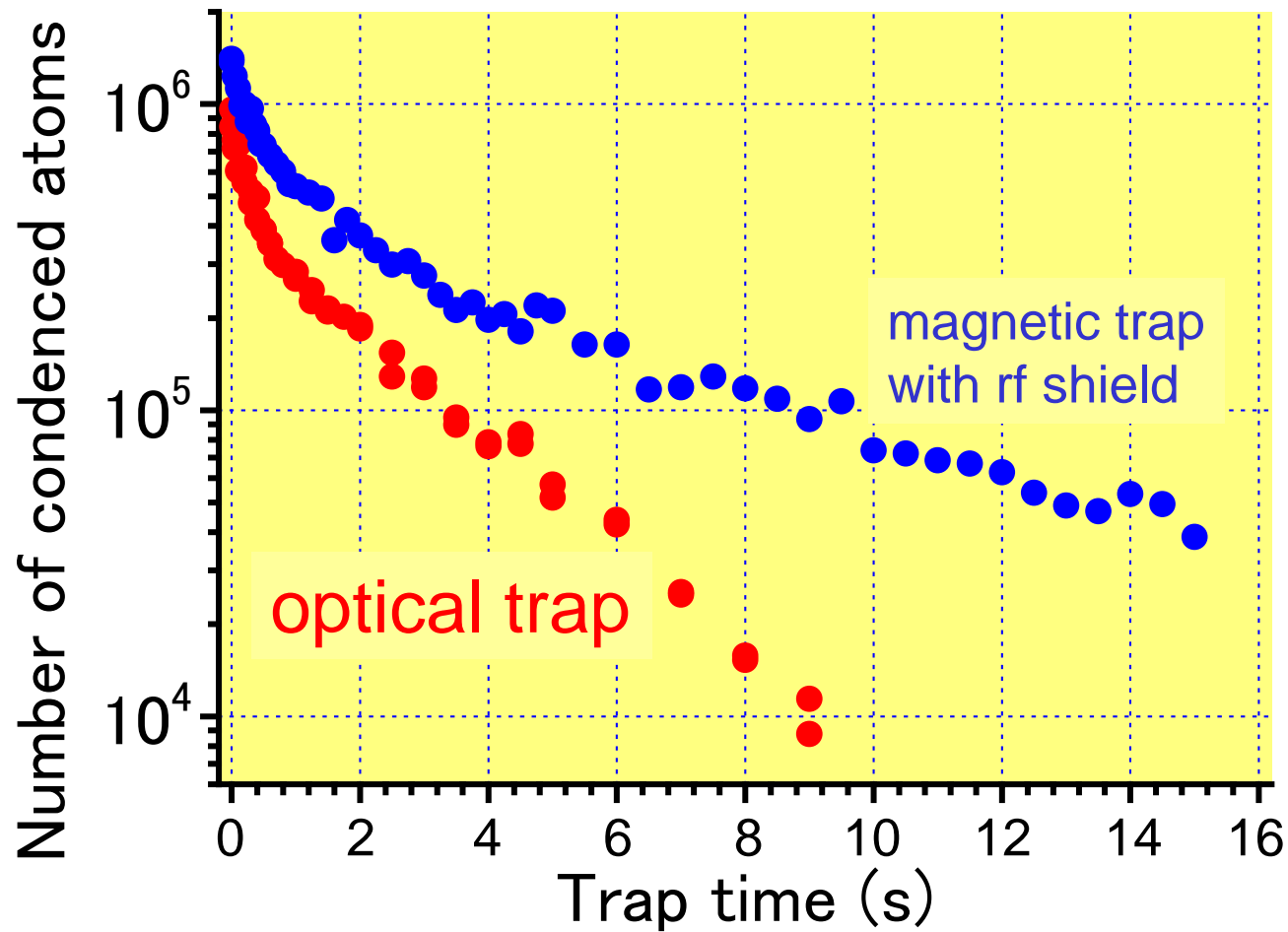
$$\propto -\frac{P}{\Delta}$$



$\alpha$  : polarizability,  $E$  : electric field  
 $P$  : laser power  
 $\Delta$  : detuning ( $f_{\text{laser}} - f_{\text{resonance}}$ )

spin degrees of freedom are liberated  
in an optical trap

# Lifetime of BEC in Optical Trap - Stretched State ( $F=2, m_F=-2$ ) -



loss rate

(in the region of  $N < 1 \times 10^5$ )

$$\tau_{\text{magnetic trap}} \sim 7 \text{ s}$$

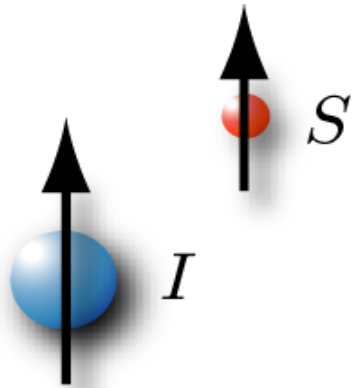
$$\tau_{\text{optical trap}} \sim 4 \text{ s}$$

photon scattering rate

$$2 \times 10^{-3} / \text{s}$$

# A short summary of atomic BEC

- Condensation not only in the momentum space but also in the coordinate space
- Typical number of atoms  $10^5$ - $10^7$ , dimension 10-100  $\mu\text{m}$ , life time < several sec.
- Internal degrees of freedom are librated in an optical trap: spinor BEC



$$F = S + L + I$$

$S$  : electron spin

$L$  : electron orbital

$I$  : nuclear spin

$^{87}\text{Rb}$ , $^{23}\text{Na}$ , $^7\text{Li}$ , $^{41}\text{K}$	$F=1, 2$
$^{85}\text{Rb}$	$F=2, 3$
$^{133}\text{Cs}$	$F=3, 4$
$^{52}\text{Cr}$	$F=3 (S=3, I=0)$
$^4\text{He}^*$ , $^{40}\text{Ca}$ , $^{174}\text{Yb}$ , $^{176}\text{Yb}$	$F=0 (S=0, I=0)$

unstable

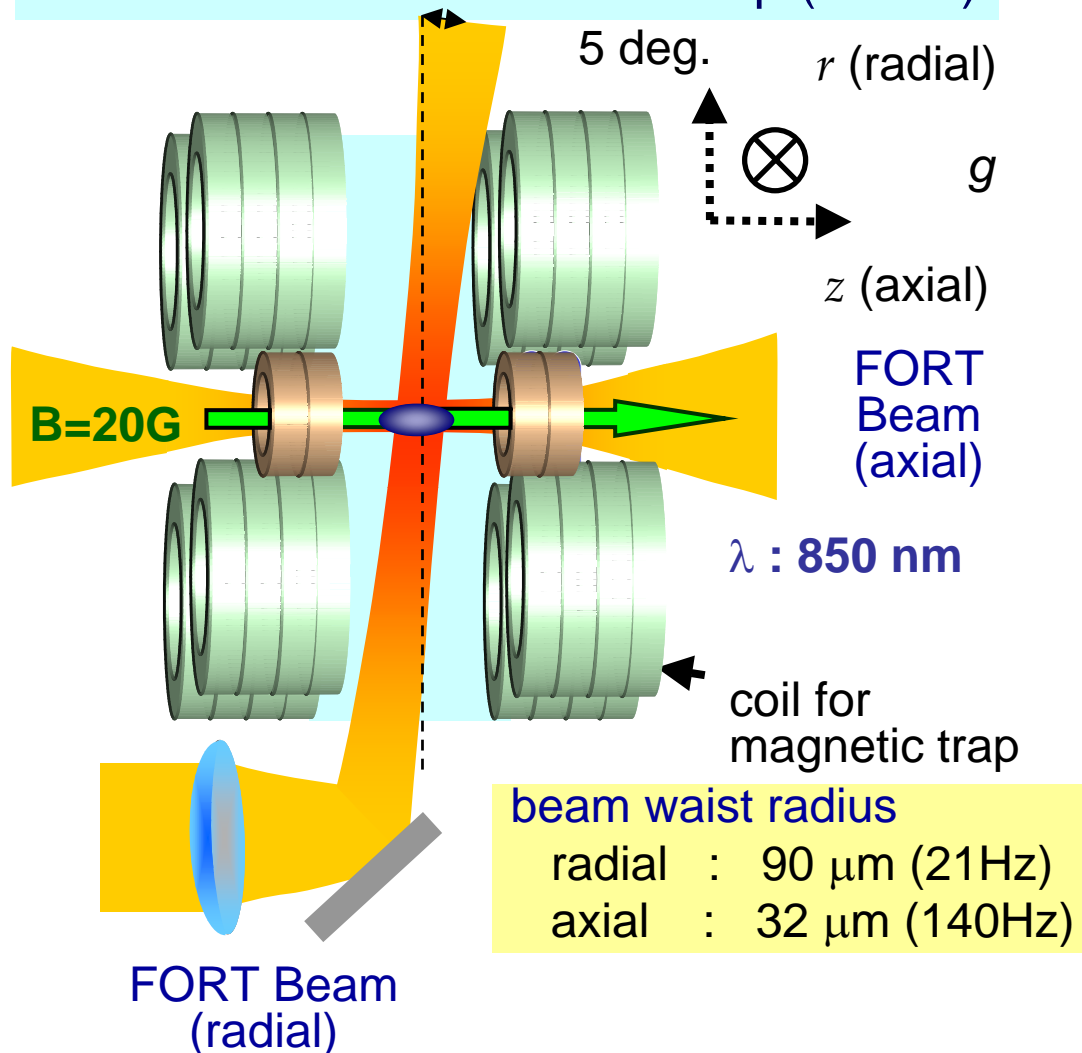
## Rb BEC with internal degrees of freedom

<sup>87</sup> Rb	high-field seeker		$m_F$	low-field seeker	
$F=2$	-2	-1	0	+1	+2
$F=1$		+1	0	-1	

- Magnetic sublevels can be coherently coupled, and their populations can be controlled.
- Scattering lengths can be controlled via Feshbach Resonance.
- Rich variety of physics
  - Spin-exchange collision, Ground-state phase,
  - Phase separation, Spin-squeezing, Quantized vortex, etc...

# Experimental setup and spin-state manipulation

## Crossed Far-Off Resonant Trap (FORT)

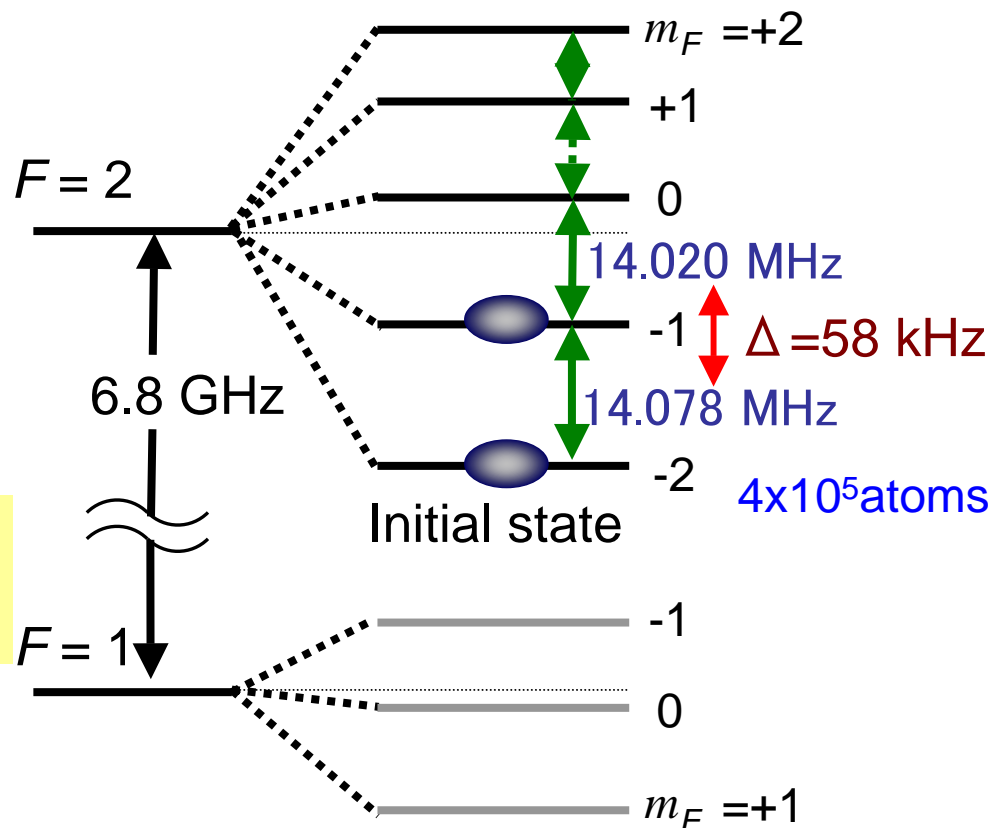


beam waist radius  
 radial :  $90 \mu\text{m}$  (21Hz)  
 axial :  $32 \mu\text{m}$  (140Hz)

Trap depth:  $\sim 1.0 \mu\text{K}$

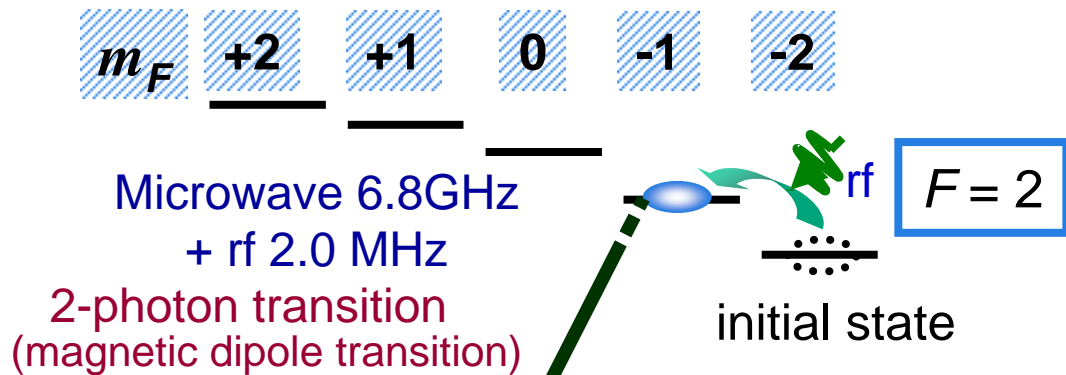
## Energy level diagram of $^{87}\text{Rb}$ (ground hyperfine states)

Zeeman splitting at  $B = 20 \text{ G}$

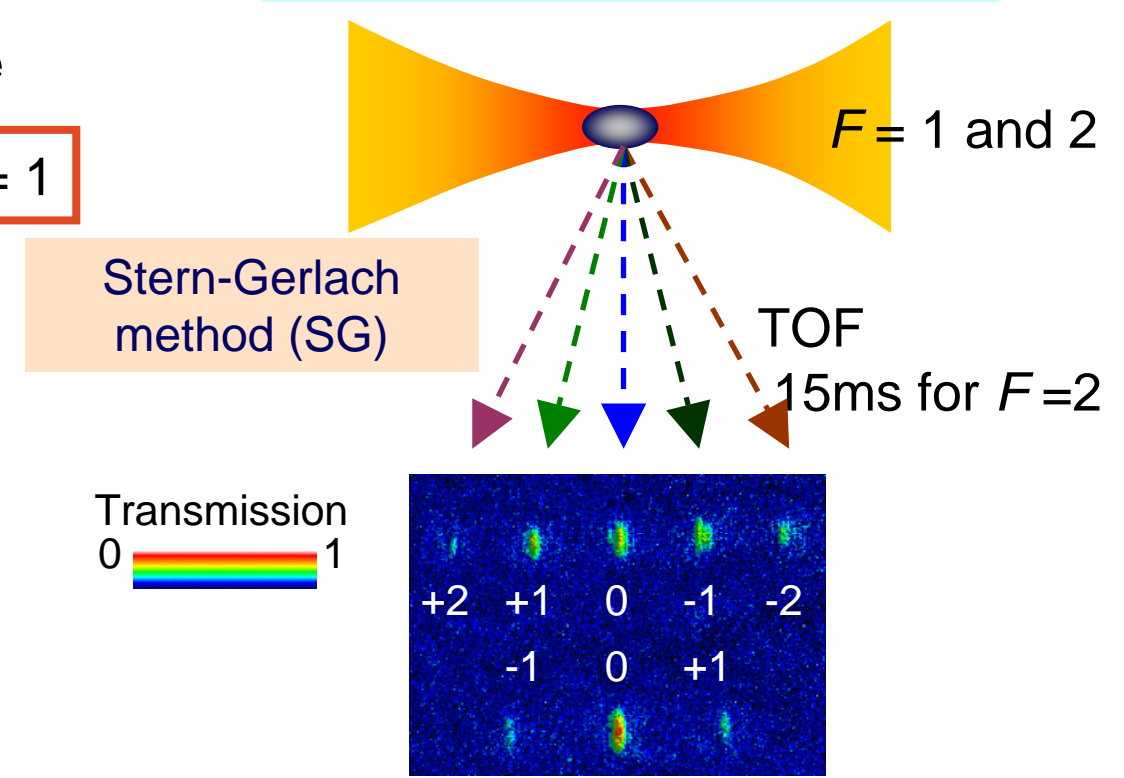
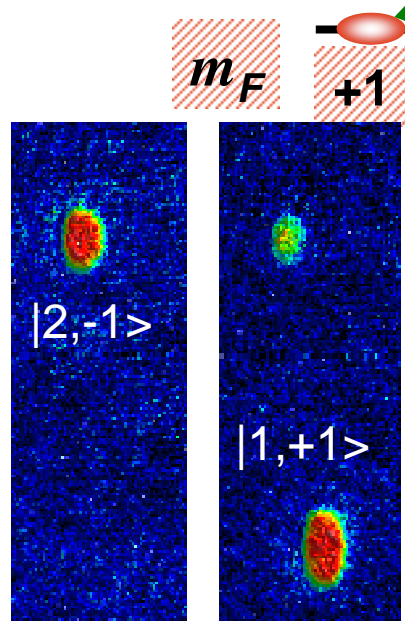


# Spin-state manipulation

Energy level diagram of  $^{87}\text{Rb}$  at 20 G

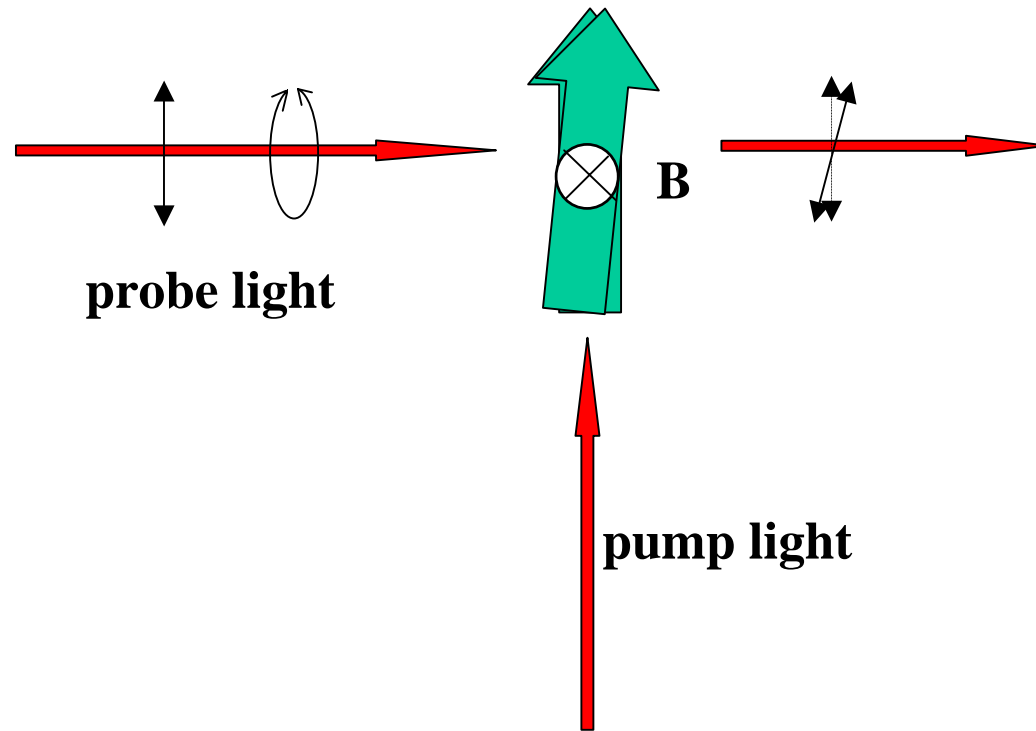
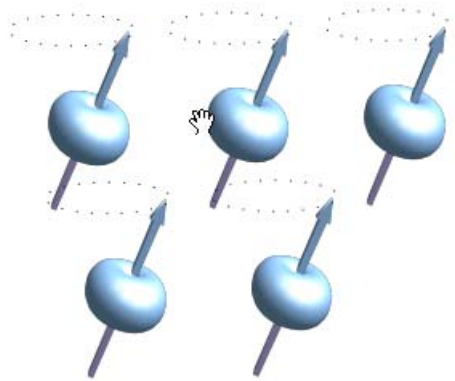


## Time evolution and imaging



18ms for  $F=1$

# Optical Magnetometer



review article: D. Budker and M. Romalis, Nature Phys. 3, 227 (2007).

# "A subfemtotesla multichannel atomic magnetometer,"

I. K. Kominis, T. W. Kornack, J. C. Allred & M. V. Romalis, Nature, Vol. 422, pp. 596-599 (2003).

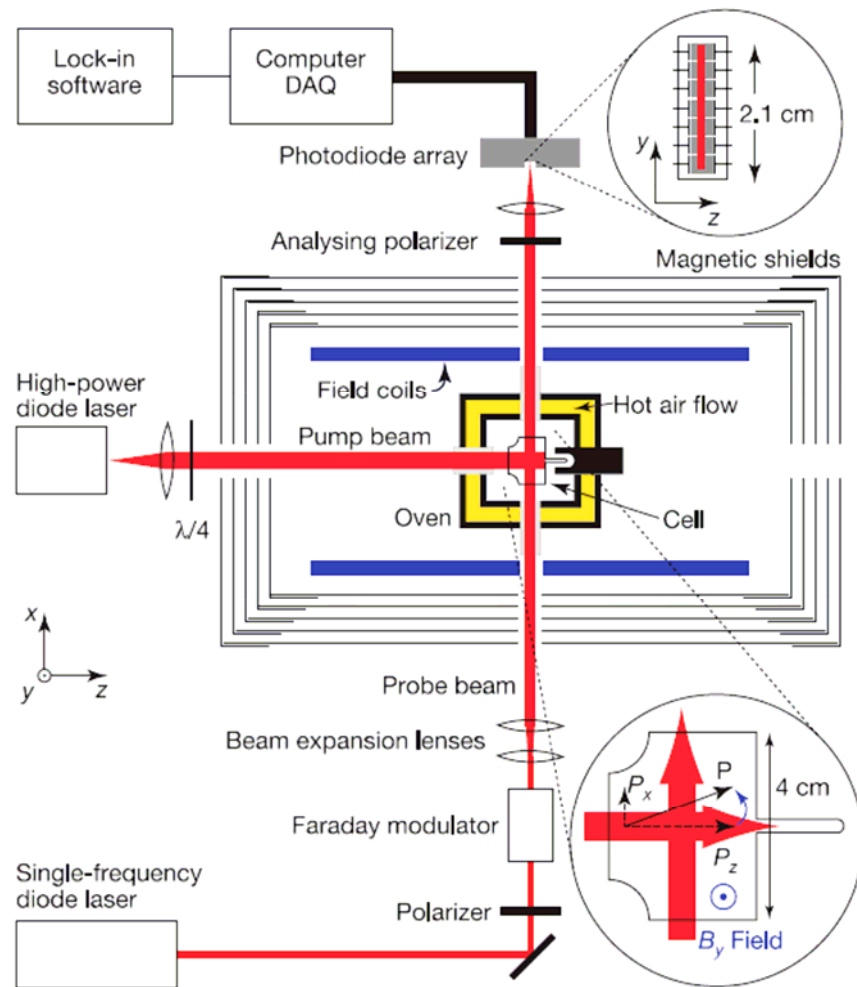


**Figure 2** Experimental set-up. The diagram shows: magnetic shields with a shielding factor of  $10^6$ ; field coils producing calibrated, uniform fields along  $\hat{x}$ ,  $\hat{y}$  and  $\hat{z}$  directions, and all five independent first-order field gradients; a T-shaped glass cell ( $3 \times 4 \times 3$  cm) with flat windows, containing a drop of K metal, 2.9 atm of  $^4\text{He}$  and 60 torr of  $\text{N}_2$ ; a double-wall oven heated to  $180^\circ\text{C}$  by flowing hot air to obtain a K atom number density of  $n \approx 6 \times 10^{13} \text{ cm}^{-3}$ ; a circularly polarized 1 W broadband diode laser ('pump' laser) tuned to the centre of the D1 line at 770 nm; a linearly polarized 100 mW single frequency laser ('probe' laser) detuned by 1 nm from the D1 resonance; a Faraday rotator modulating the plane of polarization of the probe laser with an amplitude  $\alpha \approx 0.02$  rad at a frequency  $f_{\text{mod}} = 2.9$  kHz; beam-shaping optics that produce a collimated probe beam with a cross-section of  $4 \text{ mm} \times 19 \text{ mm}$ ; a polarization analyser, orthogonal to the polarizer; a seven-element photodiode array (shown in the top inset), with element separation of 0.31 cm along the  $\hat{y}$ -direction; and a 16-bit data acquisition system using a digital seven-channel lock-in amplifier to demodulate the signal proportional to the magnetic field  $B_y$ . Bottom inset, cross-section of the T-shaped cell, showing the rotation of the K polarization  $\mathbf{P}$  into the  $\hat{x}$  direction by an applied magnetic field  $B_y$ .

$$\delta B = \frac{1}{\gamma \sqrt{n T_2 V t}} \quad \gamma = g \mu_B / \hbar (2I + 1)$$

# "A subfemtotesla multichannel atomic magnetometer,"

I. K. Kominis, T. W. Kornack, J. C. Allred & M. V. Romalis, Nature, Vol. 422, pp. 596-599 (2003).

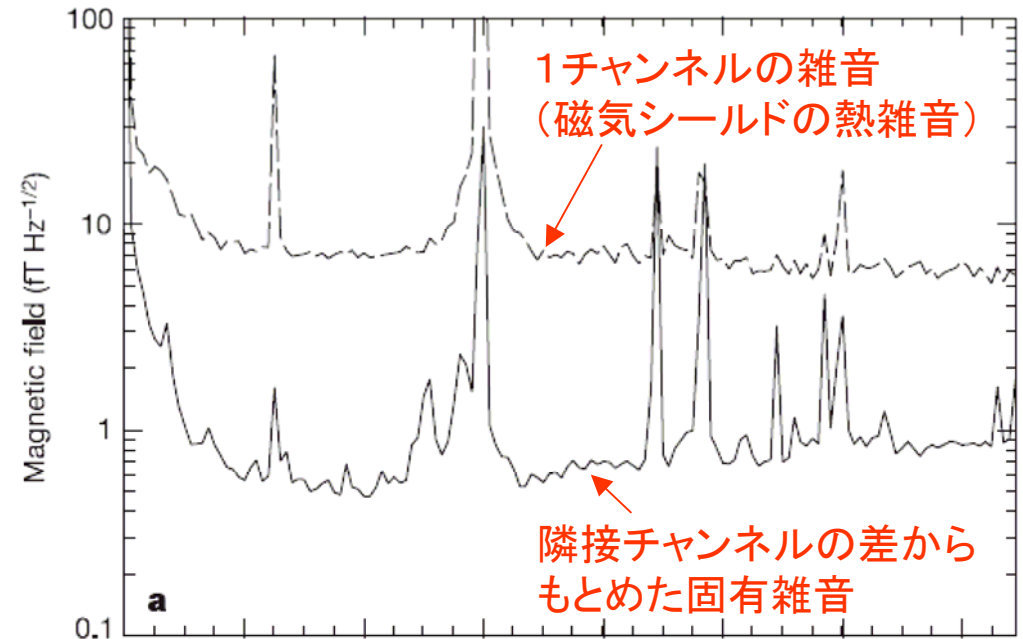
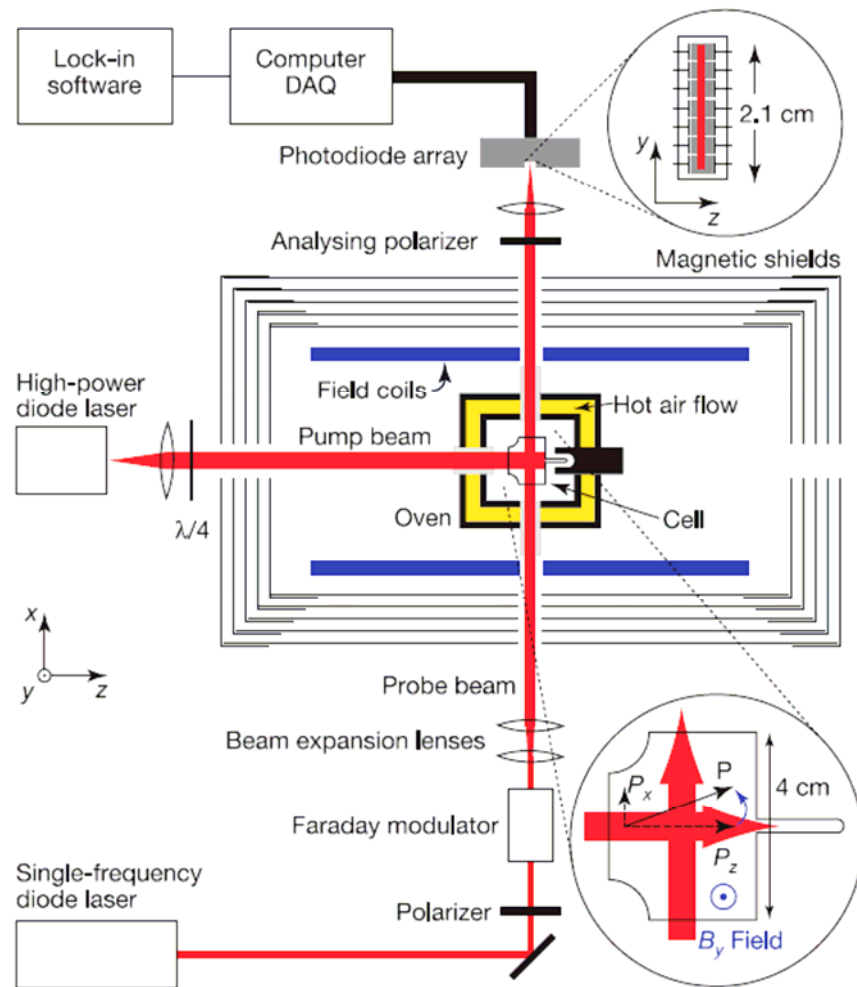
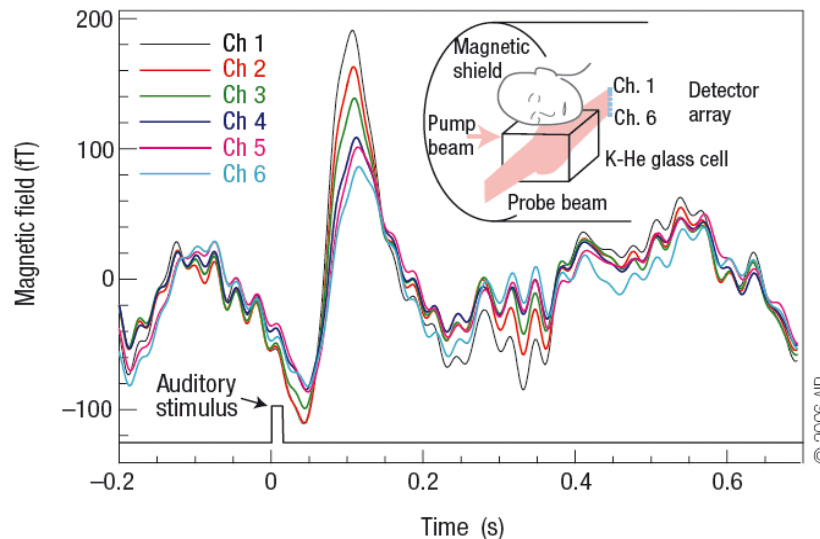


**Figure 3** Magnetic field sensitivity and bandwidth of the magnetometer. Magnetic field noise in a single channel (**a**, dashed line), and intrinsic magnetic field sensitivity of a single channel extracted from the difference between adjacent channels (**a**, solid line). The magnetic field sensitivity data are obtained by recording the response of the magnetometer for about 100 s, performing a fast Fourier transform (FFT) without windowing; and calculating r.m.s. amplitudes in 1 Hz bins. A peak due to the calibrating  $B_y$  field is seen at 25 Hz. To obtain absolute field sensitivity, we divide the magnetometer FFT by a normalized frequency-response function shown in **b** with a fit to  $A/(f^2 + B^2)^{1/2}$ ,

# Why magnetometer is important: Numerous and diverse applications

- **detection of magnetic field from brain and heart**
  - non-invasive studies of individual cortical modules in the brain
- **detection of signals of NMR and MRI**
- **detection of microparticles**
- **detection of magnetic anomalies**



Magnetic fields recorded from a brain in response to an auditory stimulation by a series of short clicks (averaged over about 600 presentations). The prominent feature at 100 ms after the stimulus is the evoked response in the auditory cortex, most clearly seen as a difference in the magnetic fields recorded by different channels. In contrast, ambient field drifts, such as those seen before the stimulus, generate similar signals in all channels. (Xia, H., Baranga, A. B., Hoff man, D. & Romalis, M. V. Magnetoencephalography with an atomic magnetometer. Appl. Phys. Lett. 89, 211104 (2006).)

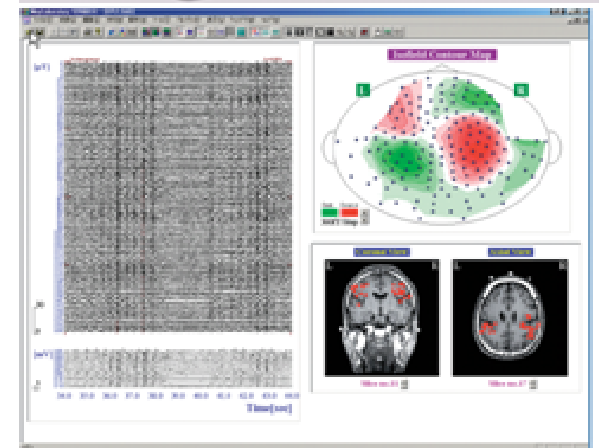
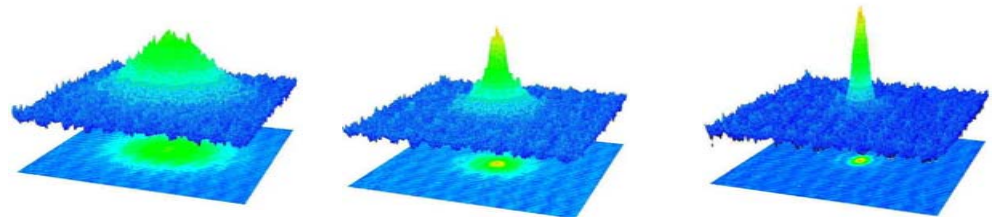


図6 臨床応用(てんかん焦点部位診断)

SQUID脳磁計(横河電機: MEGvision)

# Outline

1. Introduction
2. A brief review of atomic BEC
3. Atomic magnetometer
- 4. Magnetometer using BEC**
5. Quantum magnetometer



# "High-Resolution Magnetometry with a Spinor Bose-Einstein Condensate,"

M. Vengalattore, J. M. Higbie, S. R. Leslie, J. Guzman, L. E. Sadler, and D. M. Stamper-Kurn, Phys. Rev. Lett., Vol. 98, 200801 (2007).

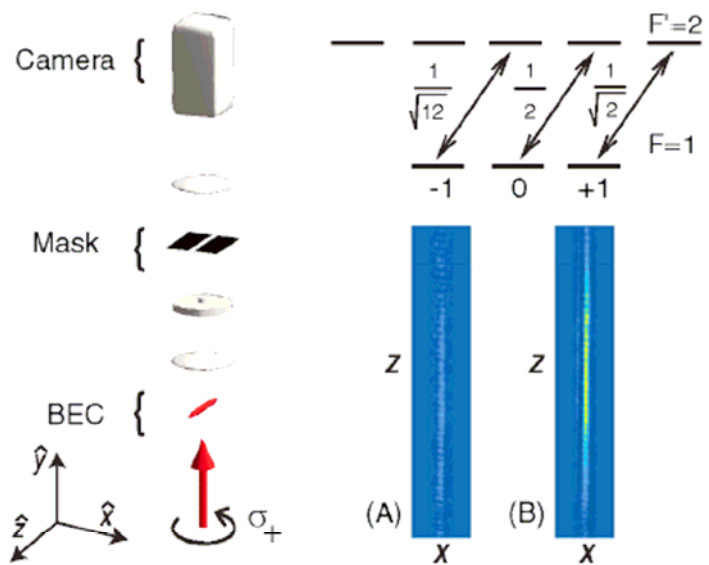


FIG. 1 (color). Imaging system for direct detection of atomic magnetization. Left: Circularly polarized probe light illuminates the trapped gas. A first lens and phase plate form a primary phase-contrast image which is selectively masked and then reimaged by a second lens onto the camera as one of  $\sim 40$  frames which form a single composite image. Top right: Clebsch-Gordan coefficients for the imaging transition. Bottom right: Sample images of a BEC (a) with the atomic spin along  $-\hat{y}$  and (b) with the spin along  $+\hat{y}$ , demonstrating the magnetization sensitivity of our technique.

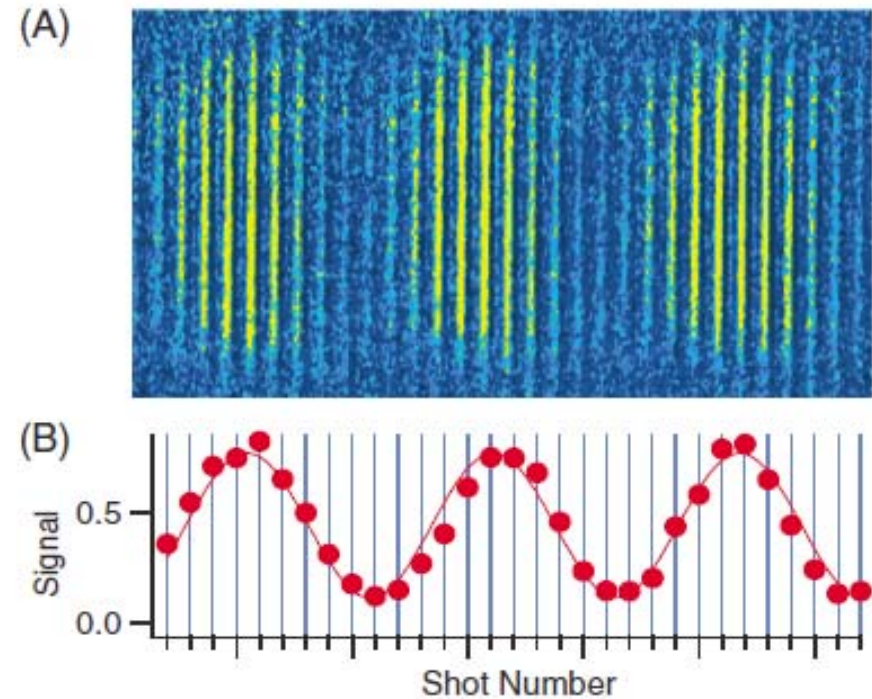


FIG. 2 (color). Direct imaging of Larmor precession of a spinor BEC through magnetization-sensitive phase-contrast imaging. Shown are 31 consecutive images each with  $325 \times 18 \mu\text{m}$  field of view. (a) Larmor precession is observed as a periodic modulation in the intensities of repeated images of a single condensate. (b) The peak signal strength oscillates at a rate which results from aliased sampling of a precisely measured  $38.097(15)$  kHz Larmor precession at a sampling rate of 20 kHz.

Direct Nondestructive Imaging of Magnetization in a Spin-1 Bose-Einstein Gas,

J. M. Higbie, L. E. Sadler, S. Inouye, A. P. Chikkatur, S.R. Leslie, K. L. Moore, V. Savalli, and D. M. Stamper-Kurn, PRL 95, 050401 (2005).

# "High-Resolution Magnetometry with a Spinor Bose-Einstein Condensate,"

M. Vengalattore, J. M. Higbie, S. R. Leslie, J. Guzman, L. E. Sadler, and D. M. Stamper-Kurn, Phys. Rev. Lett., Vol. 98, 200801 (2007).

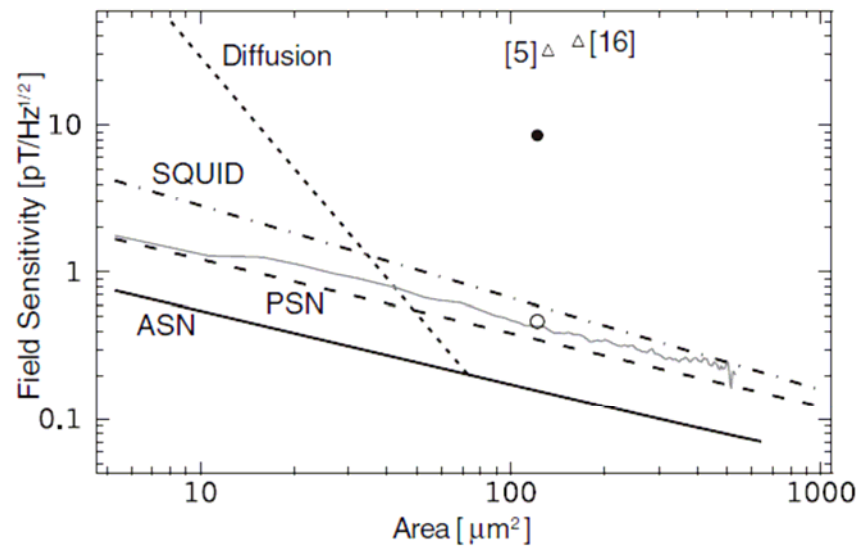


FIG. 1. Field sensitivity for repeated measurements using the spinor BEC magnetometer. Curves marked ASN (PSN) represent atom (photon) shot-noise limited sensitivities, assuming  $\tau = 250$  ms,  $D = 1$ , and the atomic column density and probe light levels for our experiment. Diffusion of magnetization limits the sensitivity for a given length scale by imposing a limit on  $\tau$  (short dashed line, assuming  $D = 1$ ). The gray line indicates the measured spatial root Allan variance; the sensitivity demonstrated in measurements of an optically induced magnetic field (see text), assuming duty cycles of  $D = 0.003$  (●) or  $D = 1$  (○), is also shown. Results are compared both to the ideal sensitivity of a quantum-limited SQUID magnetometer (dot-dashed line) and to demonstrated low-frequency sensitivities [5,16] (△).

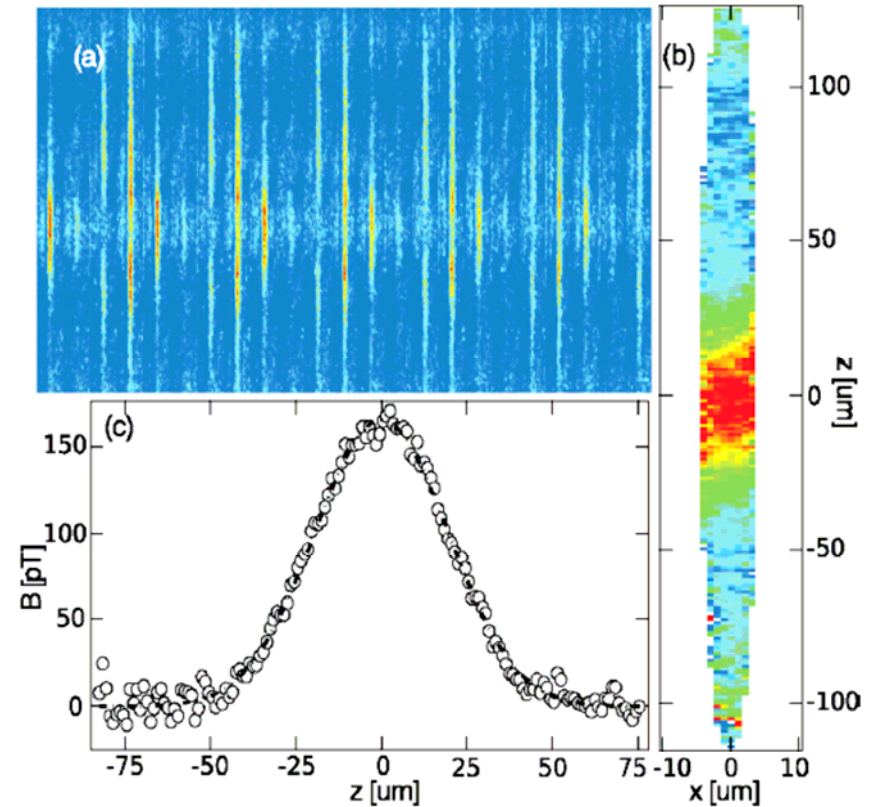
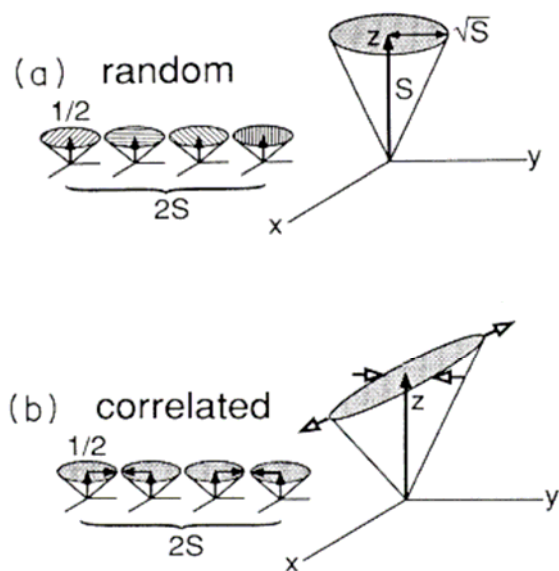


FIG. 2 (color). (a) A sequence of phase contrast images, taken at a strobe rate of 14 kHz, reveal Larmor precession as an aliased frame-to-frame oscillation of the signal. (b) The resulting 2D map of the magnetic field, obtained by a pixel-by-pixel estimation of the Larmor precession phase, reveals the optically induced local magnetic field near the condensate center. (c) The 1D phase profile precisely maps the applied field inhomogeneity with peak strength of  $166.2 \pm 1.2$  pT.

# Quantum magnetometer



“Squeezed spin states,” Masahiro Kitagawa and Masahito Ueda, Phys. Rev. A 47, 5138–5143 (1993)

## Angular momentum system

$$\vec{S} = (S_x, S_y, S_z)$$

## Cyclic commutation relation

$$[S_i, S_j] = i\epsilon_{ijk} S_k$$

$$\Rightarrow (\Delta S_i^2)(\Delta S_j^2) \geq \frac{1}{4} |\langle S_k \rangle|^2$$

For  $N$  atoms in  $m_F = F$  along the quantization axis  $z$ ,

$$S_z = FN$$

A magnetic field along  $y$  axis causes a rotation of  $S$  in  $x$ - $z$  plane. Polarization of light propagating along  $x$  will be rotated proportional to  $S_x$ . This measurement is limited by the projection noise of the atom,

$$(\Delta S_x^2) = \frac{S_z}{2} = FN / 2$$

and light shot noise of polarization measurement.

# "Sub-Projection-Noise Sensitivity in Broadband Atomic Magnetometry,"

M. Koschorreck, M. Napolitano, B. Dubost, and M. W. Mitchell, Phys. Rev. Lett., Vol. 104, 093602 (2010).

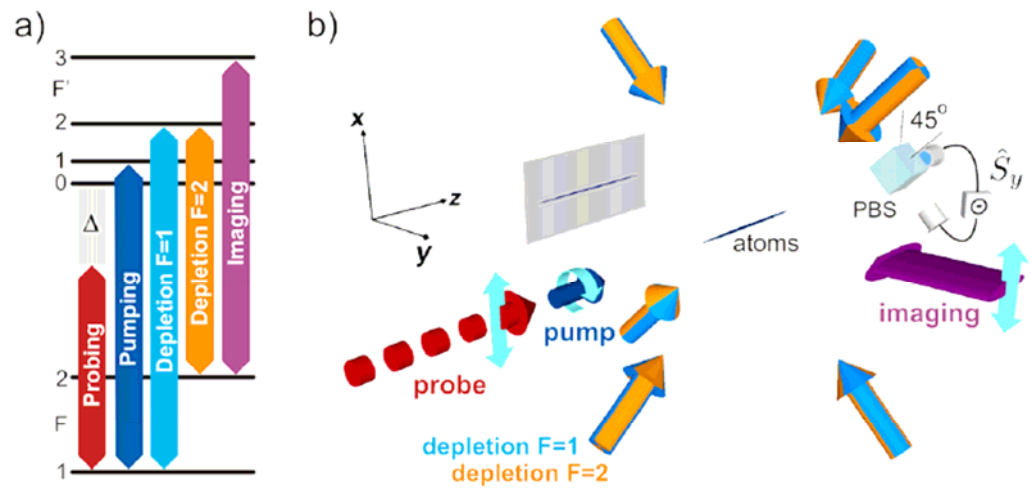


FIG. 1 (color online). (a) Atomic transitions for probing, preparation, and imaging light fields. (b) Atomic ensemble with probing, pumping, and imaging light fields. The polarimeter measures in the  $45^\circ$  basis, i.e., the Stokes component  $\hat{S}_y$ .

Laser cooled Rb atoms,  $10^6$ ,  $25\mu\text{K}$ , dipole trap  
 20 times QND measurement w/o dipole trap

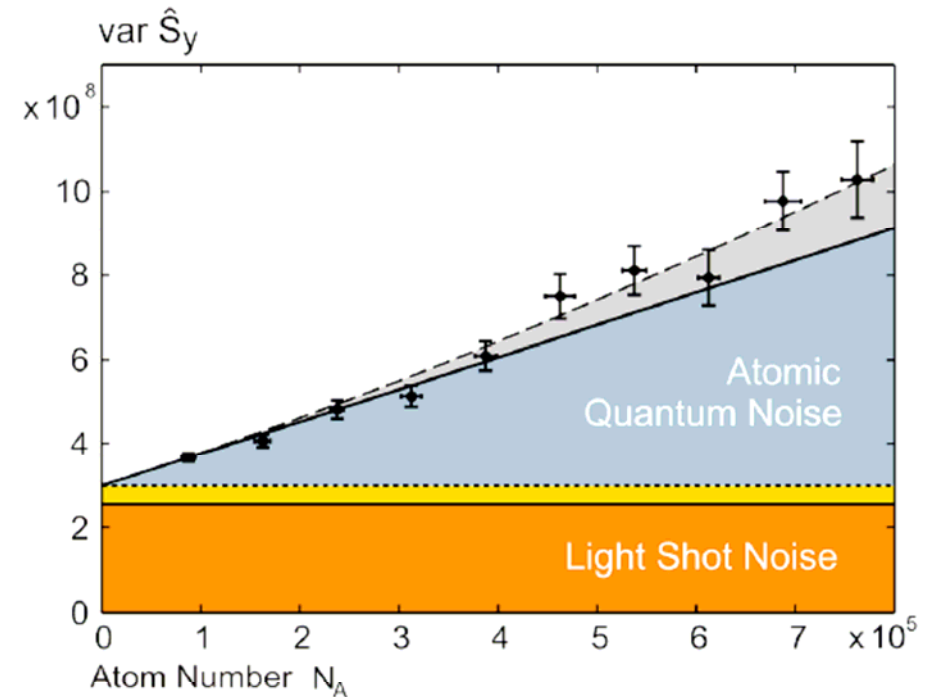


FIG. 3 (color online). Measured variance of  $\hat{S}_y$  with statistical errors for  $N_L = 10^9$  as a function of atom number. Dashed curve: theoretical curve including technical noise sources. Solid line: pure spin quantum noise. Dotted line: shot noise and technical light noise. Thin solid line: light shot noise. The electronic noise is not plotted because it is negligible for this number of photons.

“Spin Squeezing of a Cold Atomic Ensemble with the Nuclear Spin of One-Half”,  
 T. Takano, M. Fuyama, R. Namiki, and Y. Takahashi, Phys. Rev. Lett. 102, 033601 (2009).

"Squeezed-Light Optical Magnetometry," Florian Wolfgramm, Alessandro Cerè, Federica A. Beduini, Ana Predojević, Marco Koschorreck, and Morgan W. Mitchell, Phys. Rev. Lett., Vol. 105, 053601 (2010).

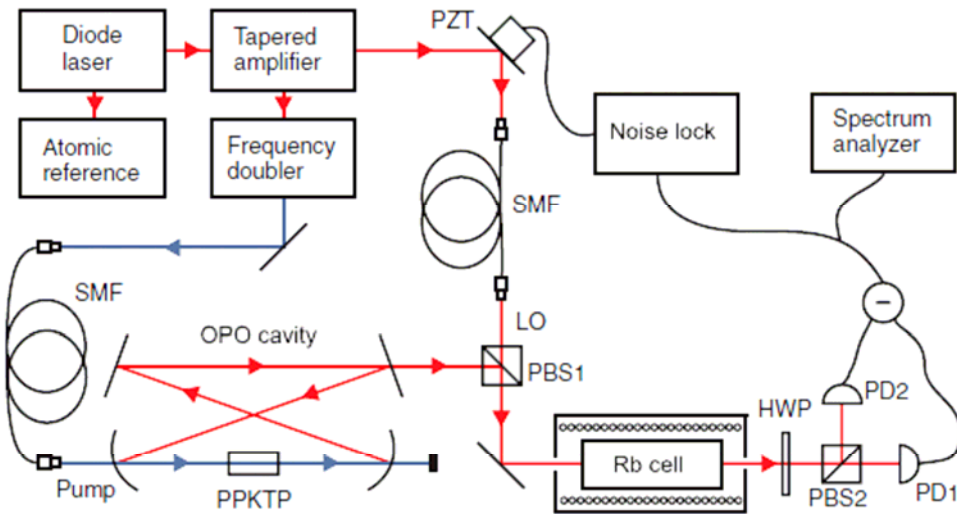


FIG. 1 (color online). Experimental apparatus. Rb cell, rubidium vapor cell with magnetic coil and magnetic shielding; OPO, optical parametric oscillator; PPKTP, phase-matched nonlinear crystal; LO, local oscillator beam; PBS, polarizing beam splitter; HWP, half-wave plate; SMF, single-mode fiber; PD, photodiode.

Hot Rb atoms, 794.7 nm, D1 line

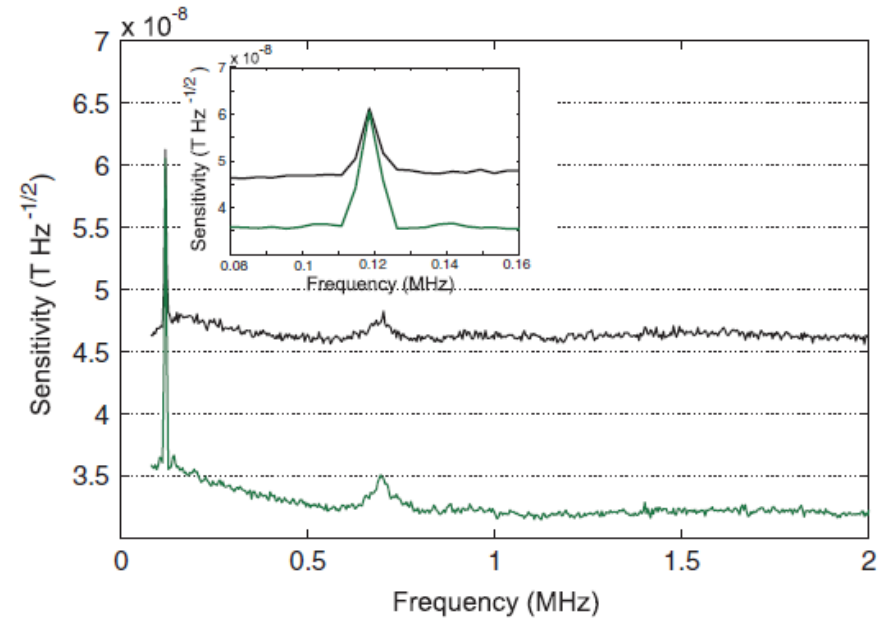


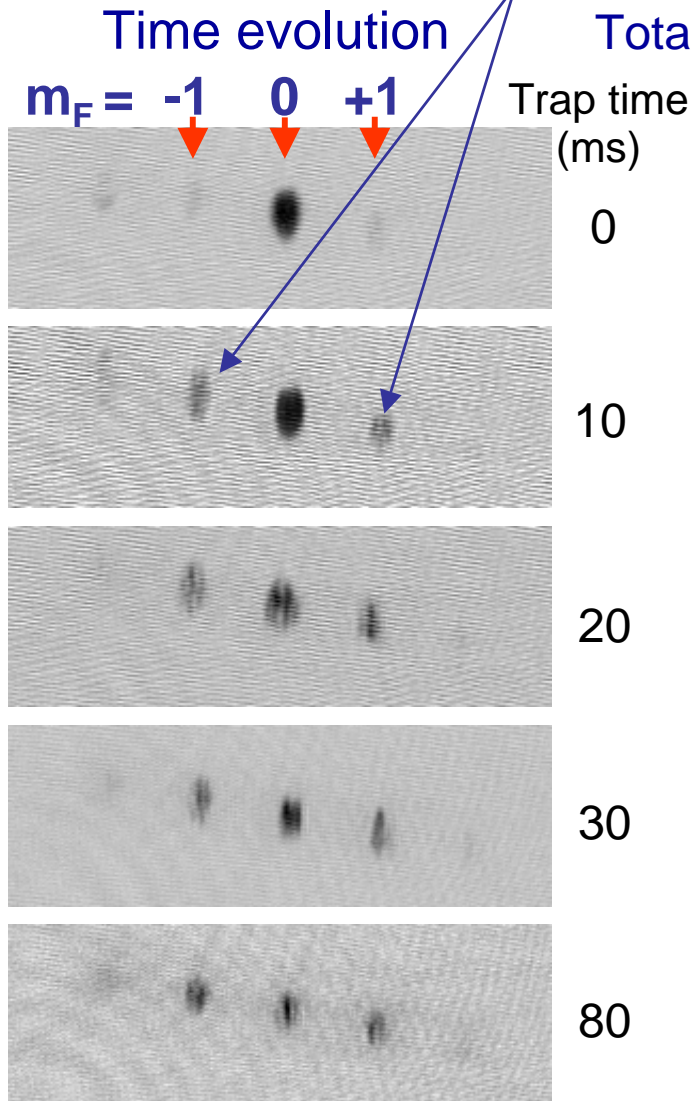
FIG. 3 (color online). Faraday rotation measurement. Power of the polarization signal as center frequency is scanned,  $RBW = 3$  kHz,  $VBW = 30$  Hz. The (upper) black curve shows the applied magnetic signal at 120 kHz above the shot-noise background of a polarized (but not squeezed) probe. The (lower) green line depicts the same signal with polarization-squeezing. A zoomed view around the calibration peak at 120 kHz is shown in the inset.

**-3.2 dB,  $3.2 \times 10^{-8}$  T/ $\sqrt{\text{Hz}}$**

# Decay of $F=2$ , $m_F=0$ BEC in OT at $B = 1.5G$

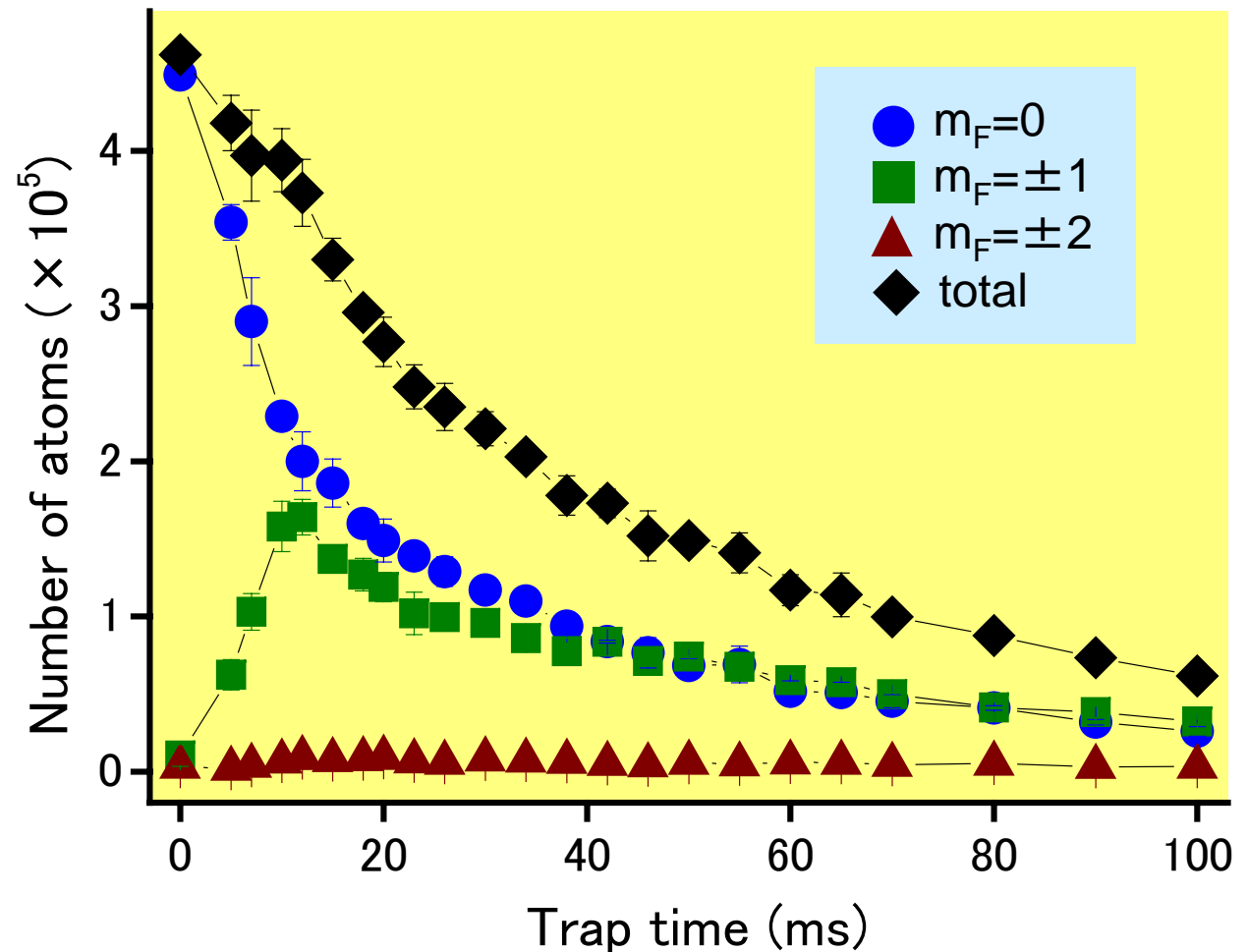
Atoms in BEC initially polarized in  $F=2$ ,  $m_F=0$  state.

$m_F=\pm 1$  components appeared during decay process.



Total-spin-conserved spin-relaxation process

Kuwamoto et al. Phys. Rev. A 69, 063604 (2004).



# Rb BEC with internal degrees of freedom

<sup>87</sup> Rb	high-field seeker		$m_F$	low-field seeker	
$F=2$	-2	-1	0	+1	+2
$F=1$		+1	0	-1	

- Ground-state phase of <sup>87</sup>Rb BEC

$$c_1 = \frac{4\pi\hbar^2}{m} \frac{a_4 - a_2}{7}$$

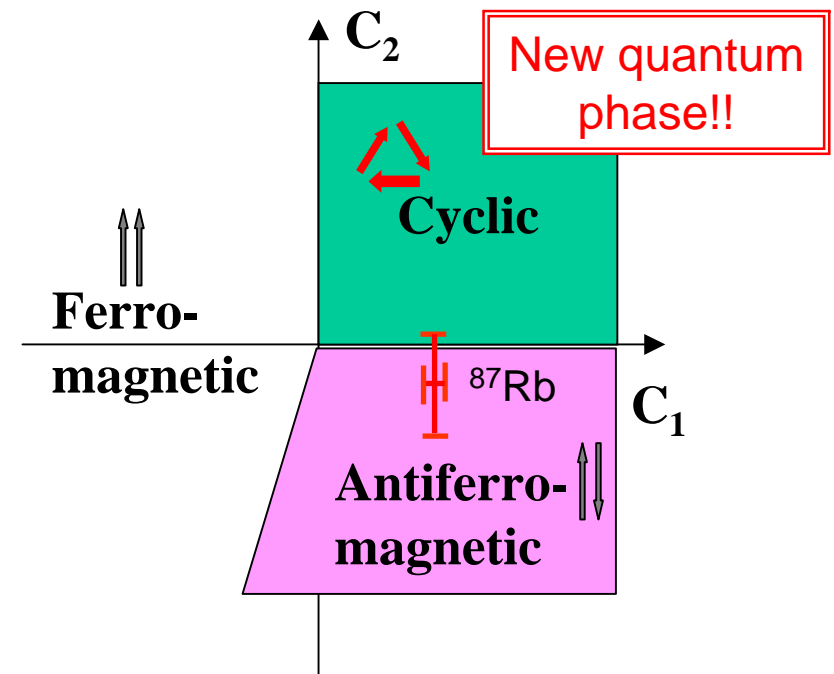
$$c_2 = \frac{4\pi\hbar^2}{m} \frac{7a_0 - 10a_2 + 3a_4}{7}$$

Measured coefficients

$$c_1 / (4\pi\hbar^2/m) = (+0.99 \pm 0.06) a_B$$

$$c_2 / (4\pi\hbar^2/m) = (-0.53 \pm 0.58) a_B$$

Widera *et al.*, *New Journal of Physics* **8**, 152 (2006)



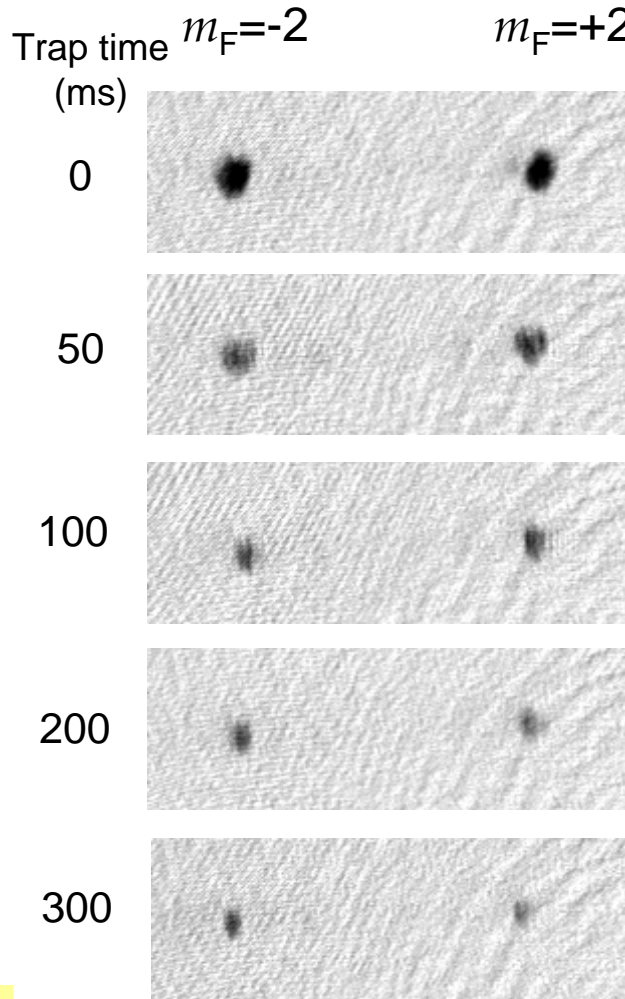
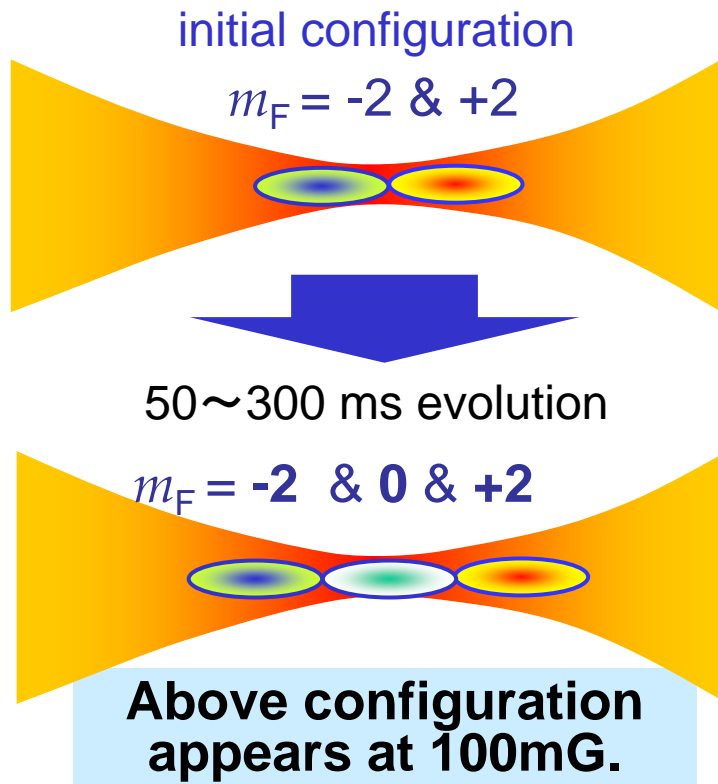
Ciobanu, Yip, & Ho, PRA 61, 033607 (2000).  
 Koashi & Ueda, PRL84, 1066 (2000).

# Evolution of $m_F = -2$ & $m_F = +2$ BEC mixture

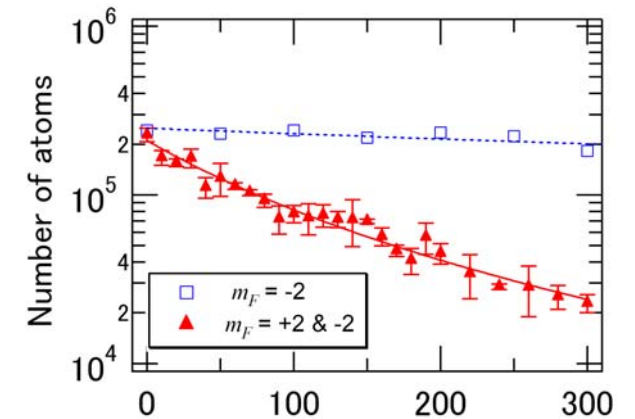
If  $F = 2$   $^{87}\text{Rb}$  spinor BEC is “cyclic”,

external magnetic field : 45mG

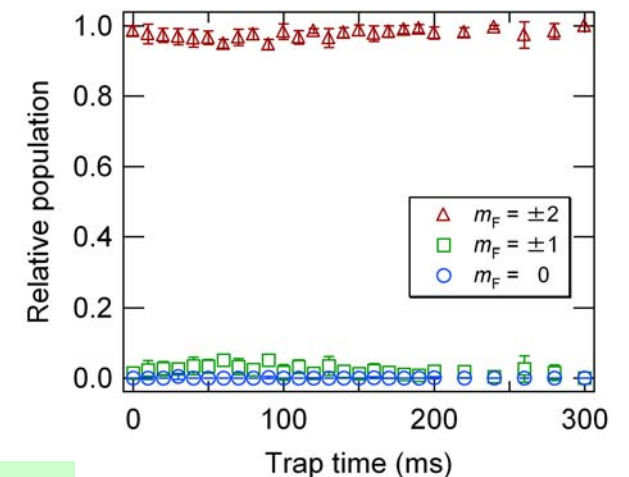
Trap time  $m_F = -2$   $m_F = +2$   
(ms)



Total remained atoms



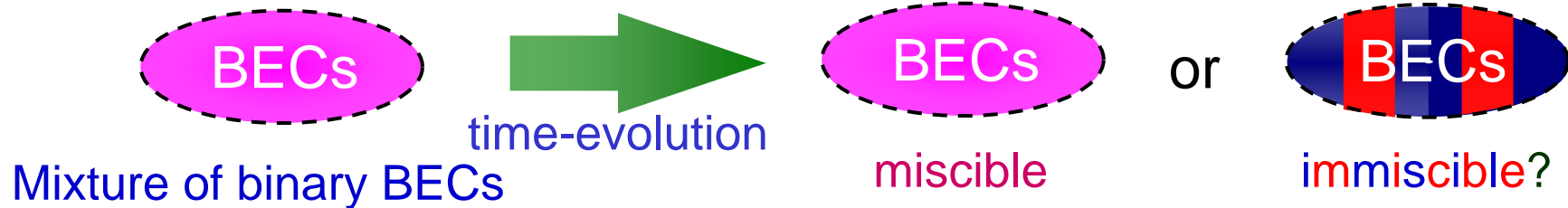
Relative population



Hiroki Sato & Masahito Ueda  
Phys.Rev.A 72, 053628 (2005)

No other components grew ...

# Miscibility of BECs



Phase-separation condition

$$a_{12}^2 > a_{11}a_{22}$$

Scattering length in (2,-1) + (1,+1) states

$$a_{22} = 95.68a_B \text{ [1]} \quad a_{11} = 100.40a_B \text{ [1]} \quad a_{21} = 97.66a_B \text{ *[2]}$$

(95.00 $a_B$  \*[2])

[1] A. Widera *et al.*, New J. Phys. **8**, 152 (2006).

Difference of scattering length gives rise to phase-separation.

[2] D.S. Hall *et al.*, PRL **81**, 1539 (1998).

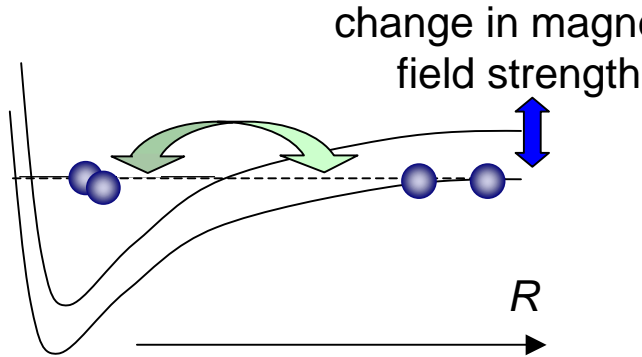
[3] K.M. Mertes *et al.*, PRL **99**, 190402 (2007).

} ( $^{87}\text{Rb}$   $|F=2, m_F= +1\rangle$  and  $|1, -1\rangle$ )

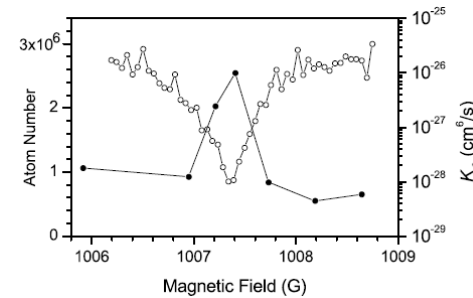
# Feshbach Resonance in mixed spin states

(1,+1)+(1,+1) @ 1007 G

resonance between atomic and molecular states

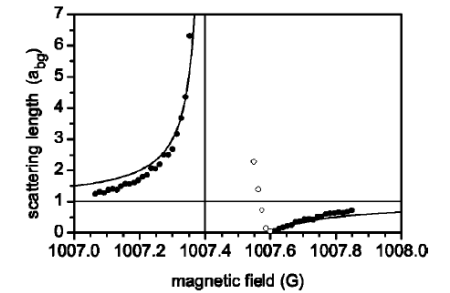


two-body loss rates



A. Merte *et al.*,  
*PRL* **89**, 283202 (2002).

scattering length



T. Voltz *et al.*,  
*PRA* **68**, 012702(R) (2003).

## Prediction

(2,+1)+(1,-1)  
@ 1.9 G

(2,-1)+(1,+1)  
@ 9.1 G

E.G. van Kempen *et al.*,  
*PRL* **88**, 093201 (2002).

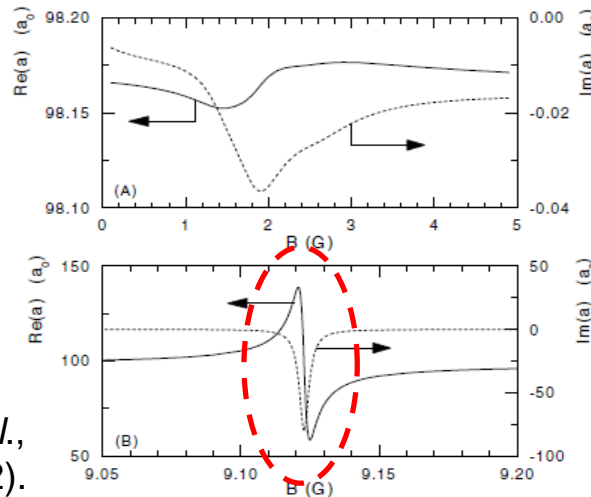


FIG. 1. (A) Real (solid line) and imaginary (dashed line) parts of the scattering length  $a(B)$  in the  $s$ -wave  $^{87}\text{Rb}$   $(2,+1) + (1,-1)$  mixed spin scattering channel, showing the presence of a Feshbach resonance at 1.9 G. The imaginary part is proportional to the summed rate coefficient  $G$  for decay into all open channels. (B) Same for Feshbach resonance in the  $(2,-1) + (1,+1)$  channel at 9.1 G.

## Experiment

(2,-1)+(1,+1)  
@ 9.09 G

M. Erhard *et al.*,  
*PRL* **69**, 032705 (2004).

Magnetic field dependence of  
two-body loss rates

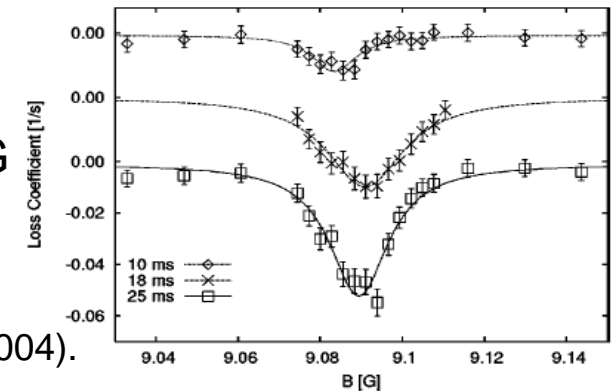
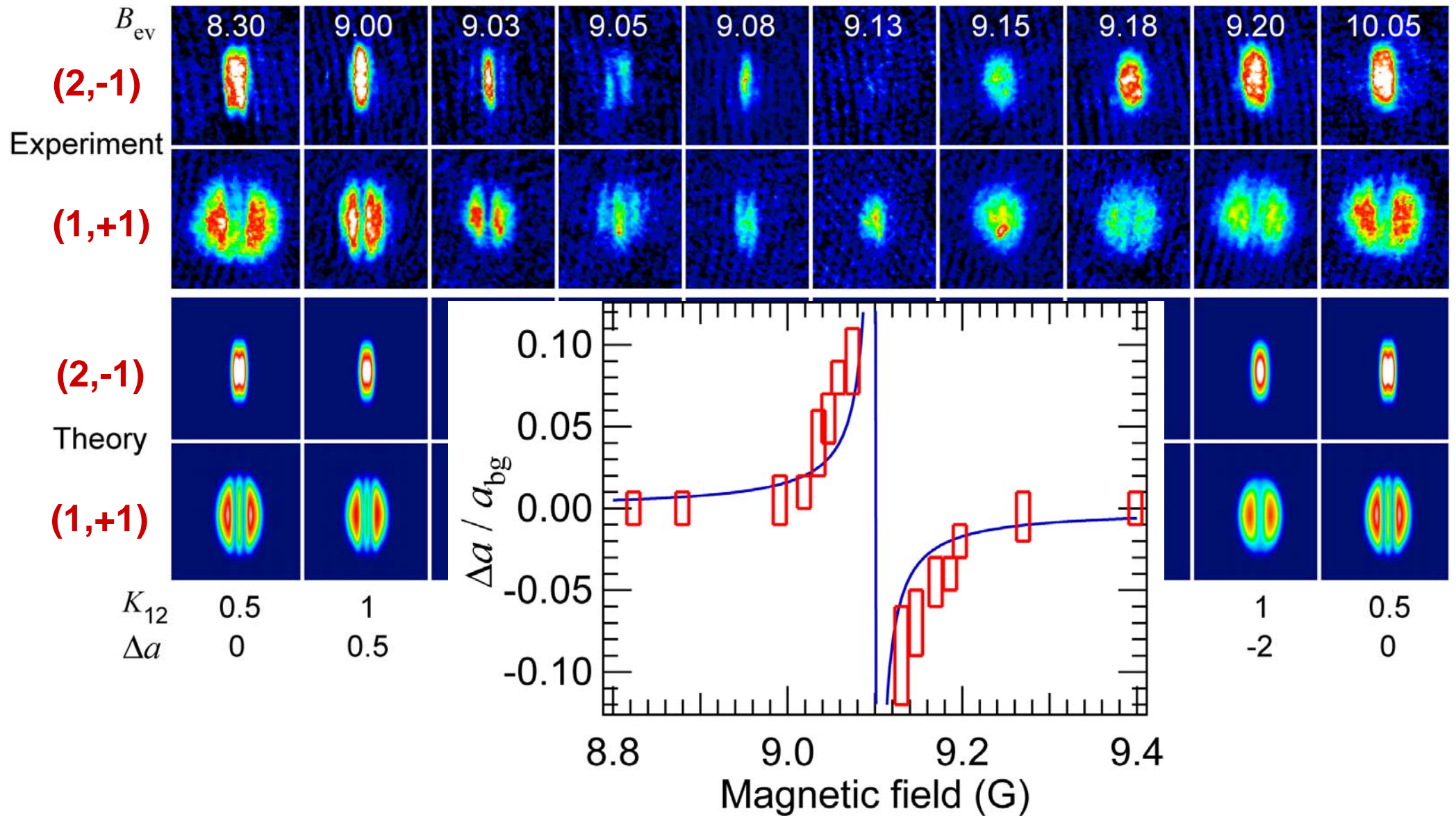
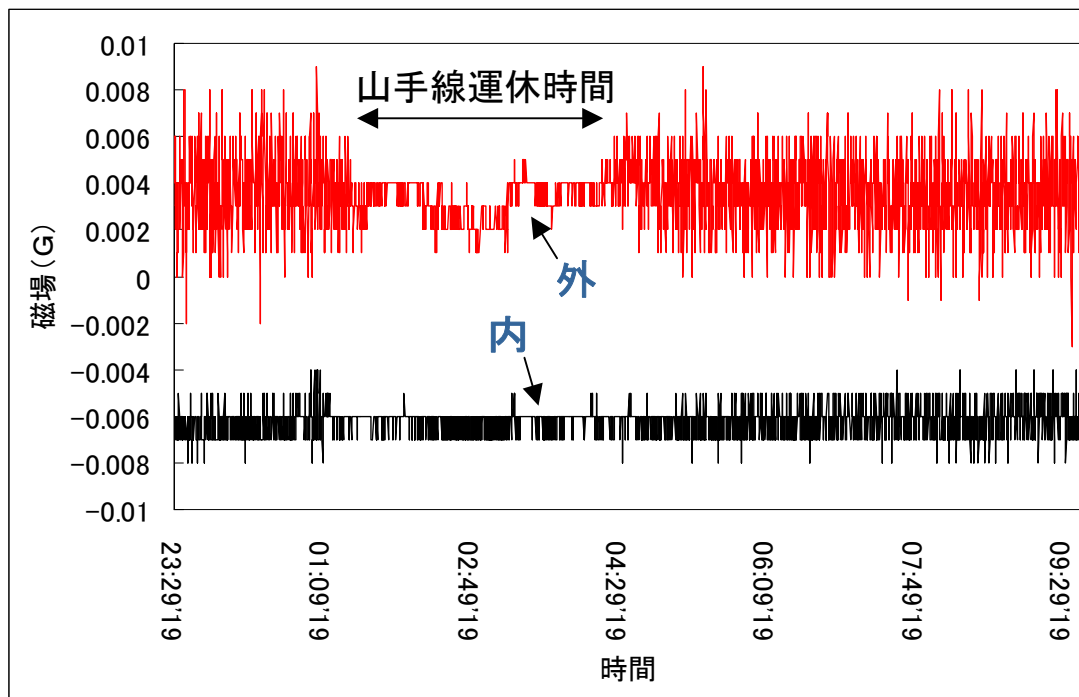
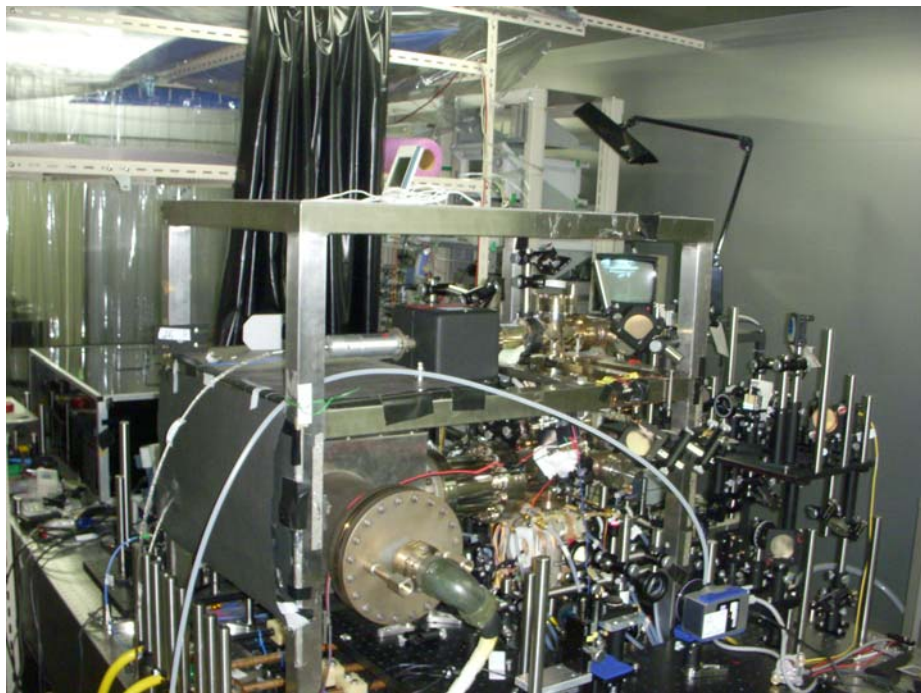


FIG. 2. Loss coefficients for a mixture of  $|2,-1\rangle$  and  $|1,+1\rangle$  states as a function of the magnetic field for hold times of 10, 18, and 25 ms. The loss coefficient is proportional to the two-body loss rate  $\bar{\gamma}$  multiplied by the hold time (see text for further explanation).

# Phase-separation near Feshbach resonance



# 現状：磁気シールドルームでBEC装置の再構築中



## 今後の研究計画

- ・F=2 Rb BECによる磁力計(バークレイはF=1)
- ・F=1とF=2のスイッチング
- ・フェッシュバハ共鳴の磁力計への応用: 磁場に敏感な現象
- ・標準量子限界を超える感度: スピンスクイーミング, 光のスクイーミング